

## A Meshless Collocation Method Based on the Differential Reproducing Kernel Approximation

Shih-Wei Yang<sup>1</sup>, Yung-Ming Wang<sup>1</sup>, Chih-Ping Wu<sup>1,2</sup> and Hsuan-Teh Hu<sup>1</sup>

**Abstract:** A differential reproducing kernel (DRK) approximation-based collocation method is developed for solving ordinary and partial differential equations governing the one- and two-dimensional problems of elastic bodies, respectively. In the conventional reproducing kernel (RK) approximation, the shape functions for the derivatives of RK approximants are determined by directly differentiating the RK approximants, and this is very time-consuming, especially for the calculations of their higher-order derivatives. Contrary to the previous differentiation manipulation, we construct a set of differential reproducing conditions to determine the shape functions for the derivatives of RK approximants. A meshless collocation method based on the present DRK approximation is developed and applied to the analysis of one-dimensional problems of elastic bars, two-dimensional potential problems, and plane elasticity problems of elastic solids to validate its accuracy and find the rate of convergence. It is shown that the present method is indeed a fully meshless approach with excellent accuracy and fast convergence rate.

**Keywords:** Meshless methods, Reproducing kernels, Collocation methods, Deformation, Stress, Elastic solids.

### 1 Introduction

Developing an efficient meshless method in computational mechanics has attracted considerable attention in recent decades. This is based on some reports which indicate that the conventional computational methods may not be suitable for the treatment of discontinuities, moving boundaries and large deformations (Liu, Jun and Zhang, 1995; Chen et al., 1996), such as finite element and finite difference methods in which formulations strongly rely on an assigned grid (or mesh). Hence, the unknown approximants in the meshless methods have been entirely constructed in terms of nodes which are randomly scattered to overcome the drawbacks of

---

<sup>1</sup> Department of Civil Engineering, National Cheng Kung University, Tainan 70101, Taiwan, ROC

<sup>2</sup> Corresponding author. Fax: +886-6-2370804, E-mail address: cpwu@mail.ncku.edu.tw

previous approaches. A comprehensive literature survey of meshless methods was undertaken by Belytschko et al. (1996), Atluri and Shen (2002), Liu (2003) and Nguyeh et al. (2008).

Liu et al. (1995) proposed the reproducing kernel (RK) particle method for numerical analysis of partial differential equations. The RK particle method was developed to address the weaknesses of smooth particle hydrodynamics (SPH) methods (Lucy, 1977; Monaghan, 1988) by introducing a correction function for kernels, such as the so-called tensile instability problem (Libersky et al., 1993). The continuous RK approximants were developed by satisfying a set of the reproducing conditions. The RK particle method has been successfully applied for the large deformation analysis of non-linear structures (Chen, Pan and Wu, 1997; Chen et al., 2000; Liew, Ng and Wu, 2002) and for the dynamic analysis of plates and shells (Zhou, Zhang and Zhang, 2005; Zhao, Liew and Ng, 2003; Liew et al., 2004; Zhao, Ng and Liew, 2004). A point collocation method based on the RK approximants was presented by Aluru (2000). It is shown that the results obtained using the RK approximation-based collocation method for several one- (1-) and two-dimensional (2D) problems of elastic solids are accurate with rapid convergence rate. Oñate, Perazzo and Miquel (2001) proposed a finite point method for the analyses of linear elastic structural problems. Jin, Li and Aluru (2005) proposed several improvements to the construction of meshless shape functions and compared several collocation schemes with the framework of the finite cloud method.

On the basis of the principle of virtual displacement (PVD), an alternative class of Galerkin-type meshless methods using the moving least squares (MLS) approximants (Lancaster and Salkauskas, 1981) has been proposed, such as the element-free Galerkin method (Belytschko, Lu and Gu, 1994; Lu, Belytschko and Gu, 1994), and the meshless local Petrov-Galerkin (MLPG) method (Atluri, Cho and Kim, 1999; Atluri and Zhu, 1998). The element-free Galerkin method has been extensively applied for the static analysis of anisotropic plates and laminates based on a first-order shear deformation theory (Belinha and Dinis, 2006) and thermo-mechanical analysis of functionally graded material plates (Dai et al., 2005). Because the computation for derivatives of unknown approximants is complicated, Atluri et al. (2004) proposed an MLPG mixed finite volume method to simplify and speed up the MLPG implementation, and this has been successfully applied to various elastic problems (Han and Atluri, 2004a, b; Han, Rajendran and Atluri, 2005). Atluri, Liu and Han (2006a) proposed an MLPG mixed collocation method using the Dirac delta function as the test function in the MLPG method, and it has been concluded that this is much more efficient than the MLPG finite volume method. Atluri, Liu and Han (2006b) further proposed an MLPG mixed difference method for solid mechanics where the generalized finite difference method was

used to approximate the derivatives of a function using the nodal values in the local domain of definition. Various elasticity problems were investigated to validate the accuracy and convergence rate of this MLPG mixed difference method.

Recently, a meshless collocation method based on the differential reproducing kernel (DRK) approximation was proposed for the three-dimensional (3D) analysis of multilayered and functionally graded (FG) plates/shells made up of smart materials (Wu, Chiu and Wang, 2008a, b, c), in which the 3D problems were reduced to 1D problems by expanding the primary field variables as a series of double Fourier functions of in-surface coordinates, the DRK approximation-based collocation method was developed and applied to the resulting system of ordinary differential equations in the thickness coordinate, and the coupling effects among the multi-fields on the static behavior of multilayered piezoelectric plates and FG magneto-electro-elastic shells/plates were mainly concerned. The novelty of the DRK approximation-based collocation method is in its modifications for the calculation of the derivatives of RK approximants, where the shape functions for the derivatives of RK approximants are determined using a set of differential reproducing conditions without directly differentiating the shape functions of the RK approximants used in the conventional RK approximation. This makes the present DRK approximation-based collocation method less time-consuming and more efficient for the calculation of the derivatives of unknown approximants. In the present paper, this method is further applied to some 1D problems of elastic bars, 2D potential problems and plane elasticity problems of elastic solids to validate its accuracy and find the rate of convergence, in which a generalized multi-dimensional formulation of DRK approximation and a 2D collocation method based on this are presented. In the implementation of this method, some guidelines to select the optimal support size and highest-order of the basis functions are discussed. In addition, the influence of uniform and random distributions of nodal points and of using different weight functions on the present results is also studied.

## **2 The DRK approximation for one-dimensional problems**

In the present DRK approximation, we focus on the determination of the shape functions for the derivatives of RK approximants using a set of differential reproducing conditions, not by differentiating the RK approximants (Liu, Jun and Zhang, 1995). In order to make a clear interpretation, we firstly simplify the derivation of the present scheme for one-dimensional problems. Afterwards, this derivation is extended to multi-dimensional problems.

## 2.1 Reproducing kernel approximants

It is assumed that there are  $NP$  discrete points randomly selected and located at  $x=x_1, x_2, \dots, x_{NP}$ , respectively, in the domain  $(\Omega)$ . The reproducing kernel approximant  $u^a(x)$  of an unknown function  $u(x)$ ,  $\forall x \in \Omega$ , is defined as

$$u^a(x) = \sum_{l=1}^{NP} \phi_l(x) \hat{u}_l, \quad (1)$$

where  $\phi_l(x) = w_a(x-x_l) C(x; x-x_l)$ ,  $C(x; x-x_l) = \mathbf{P}^T(x-x_l) \mathbf{b}(x)$ ,

$$\mathbf{P}^T(x-x_l) = [1 \quad (x-x_l) \quad (x-x_l)^2 \quad \dots \quad (x-x_l)^n],$$

$$\mathbf{b}^T(x) = [b_0(x) \quad b_1(x) \quad b_2(x) \quad \dots \quad b_n(x)];$$

$\hat{u}_l (l = 1, 2, \dots, NP)$  are the fictitious nodal values and are not the nodal values of  $u^a(x)$  in general;  $\phi_l(x)$  is the shape function for the RK approximant corresponding to nodal point at  $x=x_l$ ;  $w_a(x-x_l)$  is the weight function centered at  $x=x_l$  with a support size  $a$ ;  $C(x; x-x_l)$  is the correction function;  $b_j(x)$  ( $j = 0, 1, 2, \dots, n$ ) are the undetermined functions and will be determined by satisfying the reproducing conditions; and  $n$  is the highest-order of the basis functions.

By selecting the complete  $n^{\text{th}}$ -order polynomials as the basis functions to be reproduced, we obtain a set of reproducing conditions to determine the undetermined functions of  $b_l(x)$  in (1). The reproducing conditions are give as

$$\sum_{l=1}^{NP} \phi_l(x) x_l^m = x^m \quad m = 0, 1, 2, \dots, n. \quad (2)$$

Equation (2) represents  $(n+1)$  reproducing conditions and can be rearranged in the explicit form of

$$m = 0 : \quad \sum_{l=1}^{NP} \phi_l(x) = 1, \quad (3)$$

$$m = 1 : \quad \sum_{l=1}^{NP} \phi_l(x) (x-x_l) = x \sum_{l=1}^{NP} \phi_l(x) - \sum_{l=1}^{NP} \phi_l(x) x_l = 0, \quad (4)$$

$$m = 2 : \quad \sum_{l=1}^{NP} \phi_l(x) (x-x_l)^2 = x^2 \sum_{l=1}^{NP} \phi_l(x) - 2x \sum_{l=1}^{NP} \phi_l(x) x_l + \sum_{l=1}^{NP} \phi_l(x) x_l^2 = 0 \quad (5)$$

⋮

$$m = n : \sum_{l=1}^{NP} \phi_l(x) (x - x_l)^n = 0. \quad (6)$$

By using the expression of  $\phi_l(x)$  in (1), we can rewrite the previous reproducing conditions in the matrix form of

$$\sum_{l=1}^{NP} \mathbf{P}(x - x_l) \phi_l(x) = \sum_{l=1}^{NP} \mathbf{P}(x - x_l) w_a(x - x_l) \mathbf{P}^T(x - x_l) \mathbf{b}(x) = \mathbf{P}(0), \quad (7)$$

where  $\mathbf{P}(0) = [1 \ 0 \ 0 \ \dots \ 0]^T$ .

According to the reproducing conditions in (7), we may obtain the undetermined function matrix  $\mathbf{b}(x)$  in the following form

$$\mathbf{b}(x) = \mathbf{A}^{-1}(x) \mathbf{P}(0), \quad (8)$$

where  $\mathbf{A}(x) = \sum_{l=1}^{NP} \mathbf{P}(x - x_l) w_a(x - x_l) \mathbf{P}^T(x - x_l)$ .

Substituting (8) into (1) yields the shape functions for the RK approximant in the form of

$$\phi_l(x) = w_a(x - x_l) \mathbf{P}^T(x - x_l) \mathbf{A}^{-1}(x) \mathbf{P}(0). \quad (9)$$

It is realized from (9) that  $\phi_l(x)$  vanishes when  $x$  is not in the support of nodal point at  $x = x_l$ . The influence of the shape function in the support of each nodal point monotonically decreases as the relative distance to the nodal point increases, and this preserves the local character of the present scheme.

## 2.2 Derivatives of reproducing kernel approximants

Since the reproducing kernel approximant  $u^a(x)$  is given in (1), the first derivative of  $u^a(x)$  is therefore expressed as

$$\frac{du^a(x)}{dx} = \sum_{l=1}^{NP} \phi_l^{(1)}(x) \hat{u}_l, \quad (10)$$

where  $\phi_l^{(1)}(x)$  denotes the shape functions for the first-order derivative of the RK approximant.

In the conventional RK approximation,  $\phi_l^{(1)}(x)$  ( $l = 1, 2, \dots, NP$ ) are obtained by

directly differentiating the shape functions of the RK approximant and given as

$$\begin{aligned}\phi_l^{(1)}(x) &= \frac{\partial \phi_l(x)}{\partial x} \\ &= \frac{\partial w_a(x-x_l)}{\partial x} \mathbf{P}^T(x-x_l) \mathbf{A}^{-1}(x) \mathbf{P}(0) + w_a(x-x_l) \frac{\partial \mathbf{P}^T(x-x_l)}{\partial x} \mathbf{A}^{-1}(x) \mathbf{P}(0) \\ &\quad + w_a(x-x_l) \mathbf{P}^T(x-x_l) \frac{\partial \mathbf{A}^{-1}(x)}{\partial x} \mathbf{P}(0),\end{aligned}\tag{11}$$

where  $\frac{\partial \mathbf{A}^{-1}(x)}{\partial x} = -\mathbf{A}^{-1}(x) \frac{\partial \mathbf{A}(x)}{\partial x} \mathbf{A}^{-1}(x)$ .

It is apparent that (11) involves a lengthy expression and complicated computation, especially for calculations involving the higher-order derivatives of the RK approximant. In contrast to this, a novel approach was developed in two recent papers (Wu, Chiu and Wang, 2008a, b) in which the shape functions for the derivatives of the RK approximant are determined using a set of differential reproducing conditions, and the related derivation is given as follows.

In the DRK approximation, we expressed  $\phi_l^{(1)}(x)$  in the similar form of  $\phi_l(x)$  as follows.

$$\phi_l^{(1)}(x) = w_a(x-x_l) C_1(x; x-x_l),\tag{12}$$

where  $C_1(x; x-x_l) = \mathbf{P}^T(x-x_l) \mathbf{b}_1(x)$ ,

$$\mathbf{b}_1^T(x) = [b_0^1(x) \quad b_1^1(x) \quad b_2^1(x) \quad \cdots \quad b_n^1(x)].$$

The differential reproducing conditions for a set of complete  $n^{\text{th}}$ -order polynomials are given as

$$\sum_{l=1}^{NP} \phi_l^{(1)}(x) x_l^m = m x^{m-1} \quad m = 0, 1, 2, \dots, n.\tag{13}$$

Equation (13) can be rearranged and explicitly written as follows.

$$m = 0 : \sum_{l=1}^{NP} \phi_l^{(1)}(x) = 0,\tag{14}$$

$$m = 1 : \sum_{l=1}^{NP} \phi_l^{(1)}(x) (x-x_l) = x \sum_{l=1}^{NP} \phi_l^{(1)}(x) - \sum_{l=1}^{NP} \phi_l^{(1)}(x) x_l = -1\tag{15}$$

$$m = 2 : \sum_{l=1}^{NP} \phi_l^{(1)}(x) (x - x_l)^2 = x^2 \sum_{l=1}^{NP} \phi_l^{(1)}(x) - 2x \sum_{l=1}^{NP} \phi_l^{(1)}(x)x_l + \sum_{l=1}^{NP} \phi_l^{(1)}(x)x_l^2 = 0 \quad (16)$$

⋮

$$m = n : \sum_{l=1}^{NP} \phi_l^{(1)}(x) (x - x_l)^n = 0. \quad (17)$$

By using (12), we can rewrite the previous reproducing conditions in the matrix form of

$$\sum_{l=1}^{NP} \mathbf{P}(x - x_l) \phi_l^{(1)}(x) = \sum_{l=1}^{NP} \mathbf{P}(x - x_l) w_a(x - x_l) \mathbf{P}^T(x - x_l) \mathbf{b}_1(x) = -\mathbf{P}^{(1)}(0) \quad (18)$$

where

$$\left[ \mathbf{P}^{(1)}(0) \right] = \left. \frac{d\mathbf{P}(x - x_l)}{dx} \right|_{x=x_l} = [0 \quad -1 \quad 0 \quad \dots \quad 0]^T.$$

The undetermined function matrix  $\mathbf{b}_1(x)$  can then be obtained and given by

$$\mathbf{b}_1(x) = -\mathbf{A}^{-1}(x) \mathbf{P}^{(1)}(0). \quad (19)$$

Substituting (19) into (12) yields the shape functions for the first-order derivative of the RK approximant in the form of

$$\phi_l^{(1)}(x) = -w_a(x - x_l) \mathbf{P}^T(x - x_l) \mathbf{A}^{-1}(x) \mathbf{P}^{(1)}(0). \quad (20)$$

Carrying on the similar derivation to the  $k^{th}$ -order derivative of the RK approximant leads to

$$\frac{d^k u^a(x)}{dx^k} = \sum_{l=1}^{NP} \phi_l^{(k)}(x) \hat{u}_l, \quad (21)$$

where

$$\phi_l^{(k)}(x) = (-1)^k w_a(x - x_l) \mathbf{P}^T(x - x_l) \mathbf{A}^{-1}(x) \mathbf{P}^{(k)}(0),$$

$$\mathbf{P}^{(k)}(0) = \left. \frac{d^k \mathbf{P}(x - x_l)}{dx^k} \right|_{x=x_l}.$$

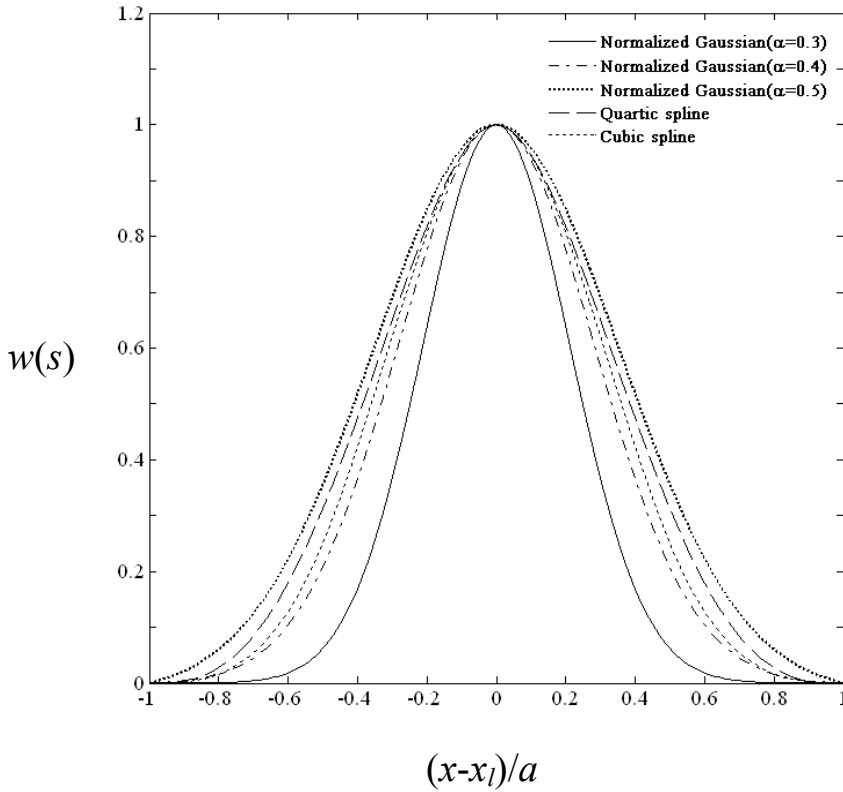


Figure 1: Various weight functions

### 2.3 Weight functions and the relative $L_2$ error norm

In implementing the present scheme, the weight functions must be selected in advance. The conventional weight functions are shown in Fig. 1 and given as

Normalized Gaussian function:

$$w(s) = \begin{cases} \frac{e^{-(s/\alpha)^2} - e^{-(1/\alpha)^2}}{1 - e^{-(1/\alpha)^2}} & \text{for } s \leq 1 \\ 0 & \text{for } s > 1 \end{cases}, \quad (22)$$

Cubic spline:

$$w(s) = \begin{cases} 6s^3 - 6s^2 + 1 & \text{for } s \leq (1/2) \\ -2s^3 + 6s^2 - 6s + 2 & \text{for } (1/2) < s < 1, \\ 0 & \text{for } s > 1 \end{cases}, \quad (23)$$

Quartic spline:

$$w(s) = \begin{cases} -3s^4 + 8s^3 - 6s^2 + 1 & \text{for } s \leq 1 \\ 0 & \text{for } s > 1 \end{cases} \quad (24)$$

where  $w_a(x - x_l) = w(s)$  and  $s = |x - x_l|/a$ .  $\alpha$  is a freely-chosen parameter, and is taken to be 0.3, 0.4, 0.5 in Fig. 1 and Tables 1-3 for comparison purposes; and the normalized Gaussian function with  $\alpha=0.3$ , which is commonly used in the literature, is adopted as the weight function in the later work of this paper due to the fact that it possesses the continuous properties of any higher-order derivative of itself and its overall performance is slightly more accurate than the other weight functions.

It is noted that a very small value of  $a$  may result in an unexpected numerical error when the calculation for the coefficients of the system matrix is performed. On the other hand, the value of  $a$  also has to be small enough to preserve the local character of the present scheme. Hence, a compromise range of the value of  $a$  will be studied later in this work to ensure the accuracy and convergence of the present scheme.

The relative  $L_2$  error norms of a certain variable and of the strain energy of an elastic body, respectively, are defined as

Relative  $L_2$  error norm of a certain variable:

$$(L_2)_u = \sqrt{\sum_{l=1}^{NP} [(u_l)_{num} - (u_l)_{exact}]^2} / \sqrt{\sum_{l=1}^{NP} (u_l)_{exact}^2}. \quad (25)$$

Relative  $L_2$  error norm of the strain energy of an elastic body:

$$(L_2)_\Pi = \sqrt{\sum_{l=1}^{NP} [(\Pi_l)_{num} - (\Pi_l)_{exact}]^2} / \sqrt{\sum_{l=1}^{NP} (\Pi_l)_{exact}^2}, \quad (26)$$

where  $\Pi$  denotes the strain energy density and is written as  $\Pi = (\sigma_x \varepsilon_x + \sigma_y \varepsilon_y + \tau_{xy} \gamma_{xy})/2$ , in which  $(\sigma_x, \sigma_y, \tau_{xy})$  are the in-plane stress components and  $(\varepsilon_x, \varepsilon_y, \gamma_{xy})$  are the in-plane strain components.

The convergence rate of the relative error norm is defined as

$$R = [\text{Log}_{10}(e_{i+1}/e_i)] / [\text{Log}_{10}(h_{i+1}/h_i)], \quad (27)$$

where  $(e_{i+1}, h_{i+1})$  and  $(e_i, h_i)$  are the relative errors and the uniform nodal spacing for the refined and coarse node distributions, respectively.

Table 1: The present DRK approximation-based collocation solutions of maximum displacement and axial force in a horizontal bar under a sinusoidally distributed load ( $n=2$ )

$\Delta x$	Weight functions	$\alpha$	Present results	$(L_2)_u$	Present results	$(L_2)_P$	
			$u(1.0)$		$P(0.0)$		
1/8	Normalized Gaussian ( $\alpha=0.3$ )	2.1 $\Delta x$	3.0228e-01	4.5e-02	6.0457e-01	4.9e-02	
	Normalized Gaussian ( $\alpha=0.4$ )	2.1 $\Delta x$	3.0289e-01	4.2e-02	6.0577e-01	4.6e-02	
	Normalized Gaussian ( $\alpha=0.5$ )	2.1 $\Delta x$	3.0380e-01	3.7e-02	6.0760e-01	4.2e-02	
	Quartic spline	2.1 $\Delta x$	3.0240e-01	4.5e-02	6.0481e-01	4.8e-02	
	Cubic spline	2.1 $\Delta x$	3.0234e-01	4.5e-02	6.0469e-01	4.8e-02	
	Normalized Gaussian ( $\alpha=0.3$ )	2.6 $\Delta x$	3.0292e-01	4.2e-02	6.0584e-01	4.6e-02	
	Normalized Gaussian ( $\alpha=0.4$ )	2.6 $\Delta x$	3.0355e-01	3.5e-02	6.0709e-01	4.2e-02	
	Normalized Gaussian ( $\alpha=0.5$ )	2.6 $\Delta x$	2.9944e-01	4.3e-02	5.9888e-01	5.3e-02	
	Quartic spline	2.6 $\Delta x$	3.0239e-01	3.6e-02	6.0477e-01	4.5e-02	
	Cubic spline	2.6 $\Delta x$	3.0355e-01	3.5e-02	6.0710e-01	4.2e-02	
	1/16	Normalized Gaussian ( $\alpha=0.3$ )	2.1 $\Delta x$	3.1425e-01	1.0e-02	6.2849e-01	1.2e-02
		Normalized Gaussian ( $\alpha=0.4$ )	2.1 $\Delta x$	3.1441e-01	9.6e-03	6.2882e-01	1.1e-02
Normalized Gaussian ( $\alpha=0.5$ )		2.1 $\Delta x$	3.1465e-01	8.4e-03	6.2929e-01	1.0e-02	
Quartic spline		2.1 $\Delta x$	3.1428e-01	1.0e-02	6.2856e-01	1.1e-02	
Cubic spline		2.1 $\Delta x$	3.1426e-01	1.0e-02	6.2853e-01	1.1e-02	
Normalized Gaussian ( $\alpha=0.3$ )		2.6 $\Delta x$	3.1442e-01	9.6e-03	6.2884e-01	1.1e-02	
	Normalized Gaussian ( $\alpha=0.4$ )	2.6 $\Delta x$	3.1456e-01	8.0e-03	6.2913e-01	1.0e-02	
	Normalized Gaussian ( $\alpha=0.5$ )	2.6 $\Delta x$	3.1352e-01	1.0e-02	6.2704e-01	1.3e-02	
	Quartic spline	2.6 $\Delta x$	3.1426e-01	8.4e-03	6.2852e-01	1.1e-02	
	Cubic spline	2.6 $\Delta x$	3.1456e-01	8.0e-03	6.2913e-01	1.0e-02	
	1/24	Normalized Gaussian ( $\alpha=0.3$ )	2.1 $\Delta x$	3.1650e-01	4.4e-03	6.3300e-01	5.0e-03
		Normalized Gaussian ( $\alpha=0.4$ )	2.1 $\Delta x$	3.1657e-01	4.1e-03	6.3314e-01	4.8e-03
Normalized Gaussian ( $\alpha=0.5$ )		2.1 $\Delta x$	3.1668e-01	3.6e-03	6.3336e-01	4.4e-03	
Quartic spline		2.1 $\Delta x$	3.1651e-01	4.3e-03	6.3303e-01	5.0e-03	
Cubic spline		2.1 $\Delta x$	3.1651e-01	4.4e-03	6.3301e-01	5.0e-03	
Normalized Gaussian ( $\alpha=0.3$ )		2.6 $\Delta x$	3.1658e-01	4.1e-03	6.3315e-01	4.8e-03	
	Normalized Gaussian ( $\alpha=0.4$ )	2.6 $\Delta x$	3.1664e-01	3.4e-03	6.3328e-01	4.4e-03	
	Normalized Gaussian ( $\alpha=0.5$ )	2.6 $\Delta x$	3.1617e-01	4.3e-03	6.3235e-01	5.7e-03	
	Quartic spline	2.6 $\Delta x$	3.1650e-01	3.6e-03	6.3301e-01	4.8e-03	
	Cubic spline	2.6 $\Delta x$	3.1664e-01	3.4e-03	6.3328e-01	4.4e-03	
	Exact solutions			3.183099e-01		6.366198e-01	

### 3 The DRK approximation for multi-dimensional problems

#### 3.1 Reproducing kernel approximants

##### 3.1.1 Two-dimensional problems

It is assumed that there are  $NP$  discrete points randomly selected and located at  $(x_l, y_l)$   $l = 1, 2, \dots, NP$ . The reproducing kernel approximant  $u^R(x, y)$  of un-

Table 2: The present DRK approximation-based collocation solutions of maximum displacement and axial force in a horizontal bar under a sinusoidally distributed load ( $n=3$ )

$\Delta x$	Weight functions	$a$	Present results	$(L_2)_u$	Present results	$(L_2)_P$	
			$u(1.0)$		$P(0.0)$		
1/8	Normalized Gaussian ( $\alpha=0.3$ )	$3.1\Delta x$	3.2643e-01	2.6e-02	6.5286e-01	2.7e-02	
	Normalized Gaussian ( $\alpha=0.4$ )	$3.1\Delta x$	3.3284e-01	4.7e-02	6.6567e-01	4.7e-02	
	Normalized Gaussian ( $\alpha=0.5$ )	$3.1\Delta x$	3.3521e-01	5.4e-02	6.7041e-01	5.4e-02	
	Quartic spline	$3.1\Delta x$	3.3360e-01	4.9e-02	6.6720e-01	4.9e-02	
	Cubic spline	$3.1\Delta x$	3.3273e-01	4.6e-02	6.6546e-01	4.6e-02	
	Normalized Gaussian ( $\alpha=0.3$ )	$3.6\Delta x$	3.3069e-01	4.0e-02	6.6138e-01	4.0e-02	
	Normalized Gaussian ( $\alpha=0.4$ )	$3.6\Delta x$	3.3720e-01	6.1e-02	6.7440e-01	6.1e-02	
	Normalized Gaussian ( $\alpha=0.5$ )	$3.6\Delta x$	3.4104e-01	7.4e-02	6.8209e-01	7.4e-02	
	Quartic spline	$3.6\Delta x$	3.3755e-01	6.2e-02	6.7511e-01	6.2e-02	
	Cubic spline	$3.6\Delta x$	3.3637e-01	5.8e-02	6.7274e-01	5.8e-02	
	1/16	Normalized Gaussian ( $\alpha=0.3$ )	$3.1\Delta x$	3.2061e-01	7.3e-03	6.4122e-01	7.3e-03
		Normalized Gaussian ( $\alpha=0.4$ )	$3.1\Delta x$	3.2225e-01	1.2e-02	6.4451e-01	1.2e-02
Normalized Gaussian ( $\alpha=0.5$ )		$3.1\Delta x$	3.2308e-01	1.5e-02	6.4615e-01	1.5e-02	
Quartic spline		$3.1\Delta x$	3.2228e-01	1.3e-02	6.4456e-01	1.3e-02	
Cubic spline		$3.1\Delta x$	3.2208e-01	1.2e-02	6.4416e-01	1.2e-02	
Normalized Gaussian ( $\alpha=0.3$ )		$3.6\Delta x$	3.2172e-01	1.1e-02	6.4343e-01	1.1e-02	
	Normalized Gaussian ( $\alpha=0.4$ )	$3.6\Delta x$	3.2378e-01	1.7e-02	6.4757e-01	1.7e-02	
	Normalized Gaussian ( $\alpha=0.5$ )	$3.6\Delta x$	3.2502e-01	2.1e-02	6.5004e-01	2.1e-02	
	Quartic spline	$3.6\Delta x$	3.2390e-01	1.8e-02	6.4779e-01	1.8e-02	
	Cubic spline	$3.6\Delta x$	3.2349e-01	1.6e-02	6.4699e-01	1.6e-02	
	1/24	Normalized Gaussian ( $\alpha=0.3$ )	$3.1\Delta x$	3.1935e-01	3.3e-03	6.3871e-01	3.3e-03
		Normalized Gaussian ( $\alpha=0.4$ )	$3.1\Delta x$	3.2009e-01	5.6e-03	6.4018e-01	5.6e-03
Normalized Gaussian ( $\alpha=0.5$ )		$3.1\Delta x$	3.2047e-01	6.8e-03	6.4095e-01	6.8e-03	
Quartic spline		$3.1\Delta x$	3.2009e-01	5.6e-03	6.4018e-01	5.6e-03	
Cubic spline		$3.1\Delta x$	3.2000e-01	5.3e-03	6.4000e-01	5.3e-03	
Normalized Gaussian ( $\alpha=0.3$ )		$3.6\Delta x$	3.1985e-02	4.9e-03	6.3970e-01	4.9e-03	
	Normalized Gaussian ( $\alpha=0.4$ )	$3.6\Delta x$	3.2081e-01	7.9e-03	6.4161e-01	7.9e-03	
	Normalized Gaussian ( $\alpha=0.5$ )	$3.6\Delta x$	3.2138e-01	9.7e-03	6.4276e-01	9.7e-03	
	Quartic spline	$3.6\Delta x$	3.2086e-01	8.0e-03	6.4172e-01	8.0e-03	
	Cubic spline	$3.6\Delta x$	3.2067e-01	7.4e-03	6.4134e-01	7.5e-03	
	Exact solutions			3.183099e-01		6.366198e-01	

known function  $u(x, y)$ ,  $\forall (x, y) \in \Omega$ , is defined as

$$u^R(x, y) = \sum_{l=1}^{NP} \psi_l(x, y) \hat{u}_l, \quad (28)$$

where  $\psi_l(x, y) = \bar{w}_a(x - x_l, y - y_l) \bar{C}(x, y; x - x_l, y - y_l)$ ,

$$\bar{C}(x, y; x - x_l, y - y_l) = \bar{\mathbf{P}}^T(x - x_l, y - y_l) \bar{\mathbf{b}}(x, y),$$

Table 3: The present DRK approximation-based collocation solutions of maximum displacement and axial force in a horizontal bar under a sinusoidally distributed load ( $n=4$ )

$\Delta x$	Weight functions	$a$	Present results	$(L_2)_u$	Present results	$(L_2)_P$
			$u(1.0)$		$P(0,0)$	
1/8	Normalized Gaussian( $\alpha=0.3$ )	4.1 $\Delta x$	3.1852e-01	4.8e-04	6.3704e-01	8.4e-04
	Normalized Gaussian( $\alpha=0.4$ )	4.1 $\Delta x$	3.1766e-01	2.0e-03	6.3531e-01	2.1e-03
	Normalized Gaussian( $\alpha=0.5$ )	4.1 $\Delta x$	3.1750e-01	2.5e-03	6.3500e-01	2.5e-03
	Quartic spline	4.1 $\Delta x$	3.1774e-01	1.7e-03	6.3548e-01	2.0e-03
	Cubic spline	4.1 $\Delta x$	3.1781e-01	1.5e-03	6.3562e-01	1.8e-03
	Normalized Gaussian( $\alpha=0.3$ )	4.6 $\Delta x$	3.1793e-01	1.2e-03	6.3586e-01	1.4e-03
	Normalized Gaussian( $\alpha=0.4$ )	4.6 $\Delta x$	3.1731e-01	3.0e-03	6.3463e-01	3.0e-03
	Normalized Gaussian( $\alpha=0.5$ )	4.6 $\Delta x$	3.1707e-01	3.8e-03	6.3414e-01	3.8e-03
	Quartic spline	4.6 $\Delta x$	3.1739e-01	2.8e-03	6.3478e-01	2.8e-03
	Cubic spline	4.6 $\Delta x$	3.1745e-01	2.6e-03	6.3490e-01	2.6e-03
1/16	Normalized Gaussian( $\alpha=0.3$ )	4.1 $\Delta x$	3.1832e-01	3.5e-05	6.3664e-01	4.7e-05
	Normalized Gaussian( $\alpha=0.4$ )	4.1 $\Delta x$	3.1825e-01	1.5e-04	6.3650e-01	1.7e-04
	Normalized Gaussian( $\alpha=0.5$ )	4.1 $\Delta x$	3.1823e-01	2.1e-04	6.3645e-01	2.4e-04
	Quartic spline	4.1 $\Delta x$	3.1826e-01	1.1e-04	6.3653e-01	1.4e-04
	Cubic spline	4.1 $\Delta x$	3.1827e-01	1.0e-04	6.3654e-01	1.3e-04
	Normalized Gaussian( $\alpha=0.3$ )	4.6 $\Delta x$	3.1827e-01	9.3e-05	6.3655e-01	1.1e-04
	Normalized Gaussian( $\alpha=0.4$ )	4.6 $\Delta x$	3.1821e-01	2.7e-04	6.3641e-01	3.0e-04
	Normalized Gaussian( $\alpha=0.5$ )	4.6 $\Delta x$	3.1812e-01	4.9e-04	6.3624e-01	5.5e-04
	Quartic spline	4.6 $\Delta x$	3.1821e-01	2.5e-04	6.3642e-01	2.8e-04
	Cubic spline	4.6 $\Delta x$	3.1822e-01	2.3e-04	6.3644e-01	2.6e-04
1/24	Normalized Gaussian( $\alpha=0.3$ )	4.1 $\Delta x$	3.1831e-01	7.6e-06	6.3662e-01	8.4e-06
	Normalized Gaussian( $\alpha=0.4$ )	4.1 $\Delta x$	3.1830e-01	2.9e-05	6.3659e-01	3.6e-05
	Normalized Gaussian( $\alpha=0.5$ )	4.1 $\Delta x$	3.1829e-01	4.2e-05	6.3658e-01	5.0e-05
	Quartic spline	4.1 $\Delta x$	3.1830e-01	2.1e-05	6.3660e-01	2.8e-05
	Cubic spline	4.1 $\Delta x$	3.1830e-01	2.0e-05	6.3660e-01	2.6e-05
	Normalized Gaussian( $\alpha=0.3$ )	4.6 $\Delta x$	3.1830e-01	1.8e-05	6.3660e-01	2.3e-05
	Normalized Gaussian( $\alpha=0.4$ )	4.6 $\Delta x$	3.1829e-01	5.3e-05	6.3657e-01	6.2e-05
	Normalized Gaussian( $\alpha=0.5$ )	4.6 $\Delta x$	3.1829e-01	3.6e-05	6.3659e-01	4.6e-05
	Quartic spline	4.6 $\Delta x$	3.1829e-01	5.0e-05	6.3658e-01	5.9e-05
	Cubic spline	4.6 $\Delta x$	3.1829e-01	4.5e-05	6.3658e-01	5.3e-05
	Exact solutions		3.183099e-01		6.366198e-01	

$$\bar{\mathbf{P}}^T(x - x_l, y - y_l) = [1 \quad (x - x_l)(y - y_l) \quad (x - x_l)^2 \quad (x - x_l)(y - y_l) \quad (y - y_l)^2 \quad \dots \quad (y - y_l)^n]'$$

$$\bar{\mathbf{b}}^T(x, y) = [\bar{b}_0(x, y) \quad \bar{b}_1(x, y) \quad \bar{b}_2(x, y) \quad \dots \quad \bar{b}_{(n+1)(n+2)/2}(x, y)]$$

By selecting a set of complete  $n^{th}$ -order polynomials as the basis functions to be reproduced, we can determine the undetermined functions of  $\bar{b}_j(x, y)$  ( $j = 0, 1, 2, \dots, (n +$

Table 4: The present DRK approximation-based collocation solutions for a 2D Laplace equation with Dirichlet boundary conditions.

Distribution of nodes ( $\Delta x$ or $\Delta y$ )	$n$	$NI$	Present results		Present results		Present results	
			$\Phi(1, 1)$	$(L_2)_\Phi$	$\Phi_{,x}(1, 1)$	$(L_2)_{\Phi_{,x}}$	$\Phi_{,y}(1, 1)$	$(L_2)_{\Phi_{,y}}$
5x5	2	9	3.984792	1.3e-02	5.854712	2.9e-02	5.854712	2.9e-02
(1/4)		11	3.986158	1.3e-02	5.859137	3.0e-02	5.859137	3.0e-02
		13	3.985982	1.2e-02	5.858672	2.5e-02	5.858672	2.5e-02
	3	17	4.000000	0.00000	6.000000	0.00000	6.000000	0.00000
		19	4.000000	0.00000	6.000000	0.00000	6.000000	0.00000
		21	4.000000	0.00000	6.000000	0.00000	6.000000	0.00000
9x9	2	9	3.992006	3.3e-03	5.897932	9.7e-03	5.897932	9.7e-03
(1/8)		11	3.992528	3.1e-03	5.899762	9.9e-03	5.899762	9.9e-03
		13	3.992591	3.0e-03	5.901043	8.1e-03	5.901043	8.1e-03
	3	17	4.000000	0.00000	6.000000	0.00000	6.000000	0.00000
		19	4.000000	0.00000	6.000000	0.00000	6.000000	0.00000
		21	4.000000	0.00000	6.000000	0.00000	6.000000	0.00000
17x17	2	9	3.995539	8.9e-04	5.939227	3.6e-03	5.939227	3.6e-03
(1/16)		11	3.995833	8.3e-04	5.941070	3.5e-03	5.941070	3.5e-03
		13	3.995892	8.0e-04	5.941396	3.2e-03	5.941396	3.2e-03
	3	17	4.000000	0.00000	6.000000	0.00000	6.000000	0.00000
		19	4.000000	0.00000	6.000000	0.00000	6.000000	0.00000
		21	4.000000	0.00000	6.000000	0.00000	6.000000	0.00000
Exact solutions			4.000000		6.000000		6.000000	

Table 5: Coordinates and the present DRK approximation-based collocation solutions for a patch test with a random distribution of 28 points.

Points	Coordinates (x,y)	Displacements		$\sigma_x$	$\sigma_y$	$\tau_{xy}$
		$u(u=x)$	$v(v=-y/4)$			
6	(4.507602, 2.522152)	4.507602	-0.63054	1	0.000000	0.000000
7	(1.530571, 0.762847)	1.530571	-0.19071	1	0.000000	0.000000
10	(3.035742, 2.442854)	3.035742	-0.61071	1	0.000000	0.000000
11	(4.19446, 0.730575)	4.19446	-0.18264	1	0.000000	0.000000
14	(5.34542, 2.787791)	5.34542	-0.69695	1	0.000000	0.000000
15	(5.755749, 1.049951)	5.755749	-0.26249	1	0.000000	0.000000
18	(3.283293, 0.589786)	3.283293	-0.14745	1	0.000000	0.000000
19	(0.831747, 0.753252)	0.831747	-0.18831	1	0.000000	0.000000
22	(0.895764, 1.848134)	0.895764	-0.46203	1	0.000000	0.000000
23	(1.54505, 1.419867)	1.54505	-0.35497	1	0.000000	0.000000

1)(n + 2)/2) in (28). The reproducing conditions are give as

$$\sum_{l=1}^{NP} \psi_l(x, y) x_l^r y_l^s = x^r y^s \quad r + s \leq n. \tag{29}$$

Equation (29) can be rearranged in the explicit form of

$r = s = 0 :$

$$\sum_{l=1}^{NP} \psi_l(x, y) = 1, \quad (30)$$

$r = 1, s = 0 :$

$$\sum_{l=1}^{NP} \psi_l(x, y) (x - x_l) = x \sum_{l=1}^{NP} \psi_l(x, y) - \sum_{l=1}^{NP} \psi_l(x, y) x_l = 0, \quad (31)$$

$r = 0, s = 1 :$

$$\sum_{l=1}^{NP} \psi_l(x, y) (y - y_l) = y \sum_{l=1}^{NP} \psi_l(x, y) - \sum_{l=1}^{NP} \psi_l(x, y) y_l = 0, \quad (32)$$

$\vdots$

$r = 0, s = n :$

$$\sum_{l=1}^{NP} \psi_l(x, y) (y - y_l)^n = 0. \quad (33)$$

By using the expression of  $\psi_l(x)$  in (28), we can rewrite the previous reproducing conditions in the matrix form of

$$\begin{aligned} & \sum_{l=1}^{NP} \bar{\mathbf{P}}(x - x_l, y - y_l) \psi_l(x, y) \\ &= \sum_{l=1}^{NP} \bar{\mathbf{P}}(x - x_l, y - y_l) \bar{w}_a(x - x_l, y - y_l) \bar{\mathbf{P}}^T(x - x_l, y - y_l) \bar{\mathbf{b}}(x, y) \\ &= \bar{\mathbf{P}}(0, 0) \end{aligned} \quad (34)$$

where  $\bar{\mathbf{P}}(0, 0) = [1 \ 0 \ 0 \ \dots \ 0]^T$ .

According to the reproducing conditions in (34), the undetermined function matrix  $\bar{\mathbf{b}}(x, y)$  can then be obtained and given by

$$\bar{\mathbf{b}}(x, y) = \bar{\mathbf{A}}^{-1}(x, y) \bar{\mathbf{P}}(0, 0), \quad (35)$$

where  $\bar{\mathbf{A}}(x, y) = \sum_{l=1}^{NP} \bar{\mathbf{P}}(x - x_l, y - y_l) \bar{w}_a(x - x_l, y - y_l) \bar{\mathbf{P}}^T(x - x_l, y - y_l)$ .

Substituting (35) into (28) yields the shape functions for the RK approximant in the form of

$$\psi_l(x, y) = \bar{w}_a(x - x_l, y - y_l) \bar{\mathbf{P}}^T(x - x_l, y - y_l) \bar{\mathbf{A}}^{-1}(x, y) \bar{\mathbf{P}}(0, 0). \quad (36)$$

### 3.1.2 Three-dimensional problems

Similar to the previous derivation, we assume that there are  $NP$  discrete points randomly selected and located at  $(x_l, y_l, z_l)$   $l = 1, 2, \dots, NP$ . The reproducing kernel approximant  $u^B(x, y, z)$  of the unknown function  $u(x, y, z)$ ,  $\forall (x, y, z) \in \Omega$ , is defined as

$$u^B(x, y, z) = \sum_{l=1}^{NP} \varphi_l(x, y, z) \hat{u}_l, \quad (37)$$

where

$$\varphi_l(x, y, z) = \tilde{w}_a(x - x_l, y - y_l, z - z_l) \tilde{\mathbf{P}}^T(x - x_l, y - y_l, z - z_l) \tilde{\mathbf{A}}^{-1}(x, y, z) \tilde{\mathbf{P}}(0, 0, 0),$$

$$\tilde{\mathbf{A}}(x, y, z) = \sum_{l=1}^{NP} \tilde{\mathbf{P}}(x - x_l, y - y_l, z - z_l) \tilde{w}_a(x - x_l, y - y_l, z - z_l) \tilde{\mathbf{P}}^T(x - x_l, y - y_l, z - z_l),$$

$$\tilde{\mathbf{P}}^T(x - x_l, y - y_l, z - z_l) = \begin{bmatrix} 1 & (x - x_l) & (y - y_l) & (z - z_l) & (x - x_l)^2 & (x - x_l)(y - y_l) & (y - y_l)^2 \\ (y - y_l)(z - z_l) & (z - z_l)^2 & (x - x_l)(z - z_l) & \cdots & (z - z_l)^n \end{bmatrix},$$

$$\tilde{\mathbf{P}}(0, 0, 0) = [1 \quad 0 \quad 0 \quad \cdots \quad 0]^T.$$

## 3.2 Derivatives of reproducing kernel approximants

### 3.2.1 Two-dimensional problems

Since the reproducing kernel approximant  $u^R(x, y)$  is given in (28), the first derivatives of  $u^R(x, y)$  are therefore expressed as

$$\frac{\partial u^R(x, y)}{\partial x} = \sum_{l=1}^{NP} \psi_l^{(x)}(x, y) \hat{u}_l, \quad (38a)$$

$$\frac{\partial u^R(x, y)}{\partial y} = \sum_{l=1}^{NP} \psi_l^{(y)}(x, y) \hat{u}_l, \quad (38b)$$

where  $\psi_l^{(x)}$  and  $\psi_l^{(y)}$  denote the shape functions for the first-order derivatives of the approximant with respect to  $x$  and  $y$ , respectively.

There is a similar derivation for determining  $\psi_l(x, y)$ , in which we express  $\psi_l^{(x)}(x, y)$  in the form of

$$\psi_l^{(x)}(x, y) = \bar{w}_a(x - x_l, y - y_l) \bar{C}_x(x, y; x - x_l, y - y_l), \quad (39)$$

where  $\bar{C}_x(x, y; x - x_l, y - y_l) = \bar{\mathbf{P}}^T(x - x_l, y - y_l) \bar{\mathbf{b}}_x(x, y)$ ,

$$\bar{\mathbf{b}}_x^T(x, y) = \left[ \bar{b}_0^{(x)}(x, y) \quad \bar{b}_1^{(x)}(x, y) \quad \bar{b}_2^{(x)}(x, y) \quad \cdots \quad \bar{b}_{(n+1)(n+2)/2}^{(x)}(x, y) \right].$$

The differential reproducing conditions for a set of complete  $n^{\text{th}}$ -order polynomials are given as

$$\sum_{l=1}^{NP} \psi_l^{(x)}(x, y) x_l^r y_l^s = r x^{r-1} y^s \quad r + s \leq n. \quad (40)$$

Equation (40) can be rearranged and explicitly written as follows.

$r = s = 0$  :

$$\sum_{l=1}^{NP} \psi_l^{(x)}(x, y) = 0, \quad (41)$$

$r = 1, s = 0$  :

$$\sum_{l=1}^{NP} \psi_l^{(x)}(x, y) (x - x_l) = x \sum_{l=1}^{NP} \psi_l^{(x)}(x, y) - \sum_{l=1}^{NP} \psi_l^{(x)}(x, y) x_l = -1, \quad (42)$$

$r = 0, s = 1$  :

$$\sum_{l=1}^{NP} \psi_l^{(x)}(x, y) (y - y_l) = y \sum_{l=1}^{NP} \psi_l^{(x)}(x, y) - \sum_{l=1}^{NP} \psi_l^{(x)}(x, y) y_l = 0, \quad (43)$$

⋮

$r = 0, s = n$  :

$$\sum_{l=1}^{NP} \psi_l^{(x)}(x, y) (y - y_l)^n = 0. \quad (44)$$

By using (39), we rewrite the previous reproducing conditions (41)-(44) in the matrix form of

$$\begin{aligned} & \sum_{l=1}^{NP} \bar{\mathbf{P}}(x-x_l, y-y_l) \boldsymbol{\psi}_l^{(x)}(x, y) \\ &= \sum_{l=1}^{NP} \bar{\mathbf{P}}(x-x_l, y-y_l) \bar{w}_a(x-x_l, y-y_l) \bar{\mathbf{P}}^T(x-x_l, y-y_l) \bar{\mathbf{b}}_x(x, y) \\ &= (-1) \frac{\partial \bar{\mathbf{P}}}{\partial x}(0, 0) \end{aligned} \quad (45)$$

where  $\frac{\partial \bar{\mathbf{P}}}{\partial x}(0, 0) = [0 \quad -1 \quad 0 \quad \cdots \quad 0]^T$ .

According to the reproducing conditions in (45), the undetermined function matrix  $\bar{\mathbf{b}}_x(x, y)$  can then be obtained and given by

$$\bar{\mathbf{b}}_x(x, y) = (-1) \bar{\mathbf{A}}^{-1}(x, y) \frac{\partial \bar{\mathbf{P}}}{\partial x}(0, 0). \quad (46)$$

Substituting (46) into (28) yields the shape functions for  $(\partial u^R / \partial x)$  in the form of

$$\boldsymbol{\psi}_l^{(x)}(x, y) = (-1) \bar{w}_a(x-x_l, y-y_l) \bar{\mathbf{P}}^T(x-x_l, y-y_l) \bar{\mathbf{A}}^{-1}(x, y) \frac{\partial \bar{\mathbf{P}}}{\partial x}(0, 0). \quad (47)$$

Similarly, we can express  $\boldsymbol{\psi}_l^{(y)}$  as

$$\boldsymbol{\psi}_l^{(y)}(x, y) = (-1) \bar{w}_a(x-x_l, y-y_l) \bar{\mathbf{P}}^T(x-x_l, y-y_l) \bar{\mathbf{A}}^{-1}(x, y) \frac{\partial \bar{\mathbf{P}}}{\partial y}(0, 0). \quad (48)$$

Carrying out the same derivation for the higher-order derivatives of the RK approximant leads to

$$\frac{\partial^{p+q} u^R(x, y)}{\partial x^p \partial y^q} = \sum_{l=1}^{NP} \boldsymbol{\psi}_l^{\overbrace{(xx \cdots xy \cdots)}^{p \quad q}}(x, y) \hat{u}_l, \quad (49)$$

where

$$\begin{aligned} & \boldsymbol{\psi}_l^{\overbrace{(xx \cdots xy \cdots)}^{p \quad q}}(x, y) = \\ & (-1)^{p+q} \bar{w}_a(x-x_l, y-y_l) \bar{\mathbf{P}}^T(x-x_l, y-y_l) \bar{\mathbf{A}}^{-1}(x, y) \frac{\partial^{p+q} \bar{\mathbf{P}}}{\partial x^p \partial y^q}(0, 0). \end{aligned}$$

### 3.2.2 Three-dimensional problems

Similarly, the higher-order derivatives of the reproducing kernel approximant for three-dimensional problems are

$$\frac{\partial^{p+q+t} u^B(x, y, z)}{\partial x^p \partial y^q \partial z^t} = \sum_{l=1}^{NP} \varphi_l^{\overbrace{(xx \dots yy \dots zz \dots)}^{p \quad q \quad t}}(x, y, z) \hat{u}_l, \quad (50)$$

where

$$\begin{aligned} & \varphi_l^{\overbrace{(xx \dots yy \dots zz \dots)}^{p \quad q \quad t}}(x, y, z) \\ &= (-1)^{p+q+t} \tilde{w}_a(x-x_l, y-y_l, z-z_l) \tilde{\mathbf{P}}^T(x-x_l, y-y_l, z-z_l) \tilde{\mathbf{A}}^{-1}(x, y, z) \\ & \frac{\partial^{p+q+t} \tilde{\mathbf{P}}}{\partial x^p \partial y^q \partial z^t}(0, 0, 0). \end{aligned}$$

## 4 Applications

A point collocation method based on the present DRK approximation is formulated and applied to a variety of structural problems in the following illustrative examples. The present solutions of the DRK approximation-based collocation method are compared with the exact solutions available in the literature to validate its accuracy and find the rate of convergence.

### 4.1 Static analysis of bars

The static analysis of a uniform bar with homogeneous isotropic material properties and under a sinusoidally distributed load ( $f(x)$ ) in the  $x$  direction, is considered and shown in Fig. 2. The edge at the left hand side is clamped and at the right hand side is free. The governing equation of the uniform bar is given by

$$AE \frac{d^2 u(x)}{dx^2} + f(x) = 0 \text{ in } 0 < x < L, \quad (51)$$

where  $f(x) = f_0 \sin(\pi x/L)$ ,  $AE$  is the axial rigidity of the beam, and  $L$  is the length of the bar.

Equation (51) is normalized and rewritten as

$$\frac{d^2 \bar{u}}{d\bar{x}^2} + \bar{f}(\bar{x}) = 0 \text{ in } 0 < \bar{x} < 1 \quad (52)$$

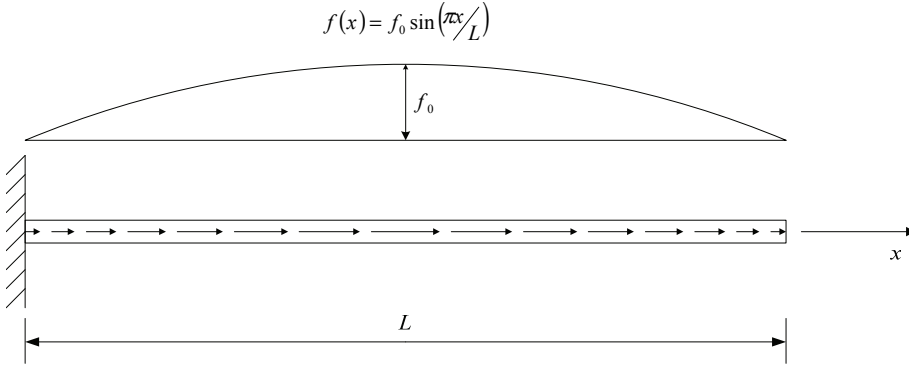


Figure 2: The configuration, coordinates and loading condition of a uniform bar

where  $\bar{x} = x/L$ ,  $\bar{u} = AE u / f_0 L^2$ ,  $\bar{f}(\bar{x}) = f(x) / f_0$  (or  $\bar{f}(\bar{x}) = \sin(\pi\bar{x})$ ),  $f_0$  is a reference magnitude of the distributed load.

The boundary conditions in the dimensionless form are given as

$$\bar{u} = 0 \text{ at } \bar{x} = 0, \tag{53a}$$

$$AE \frac{d\bar{u}}{d\bar{x}} = 0 \text{ at } \bar{x} = 1. \tag{53b}$$

Randomly selecting  $NP$  sampling points and applying the present DRK approximation-based collocation method to (52) at each nodal point in the bar domain leads to

$$\sum_{l=1}^{NP} \phi_l^{(2)}(\bar{x}_k) \hat{u}_l = -\sin(\pi\bar{x}_k) \text{ for } k = 1, 2, 3, \dots, NP, \tag{54}$$

Similarly, applying the present method to the edge conditions leads to

$$\sum_{l=1}^{NP} \phi_l(0) \hat{u}_l = 0, \tag{55a}$$

$$\sum_{l=1}^{NP} \phi_l^{(1)}(1) \hat{u}_l = 0. \tag{55b}$$

The set of equations (54) and (55) represents a mathematical system consisting of  $(NP+2)$  simultaneously algebraic equations in terms of  $NP$  unknowns. The present solutions can then be obtained by solving the previous set of algebraic equations using a weighted least squares method with a weight number of 10,000 for the

essential boundary condition (55a), 100 for the natural boundary condition (55b), and 1 for Euler equations (54). The present solution is validated by the exact solutions of horizontal displacement ( $[\bar{u}(\bar{x})]_{exact} = \frac{1}{\pi^2} \sin(\pi\bar{x}) + \frac{\bar{x}}{\pi}$ ) and axial force ( $[\bar{P}(\bar{x})]_{exact} = \frac{1}{\pi} \cos(\pi\bar{x}) + \frac{1}{\pi}$ ).

Tables 1-3 show the present solutions of maximum axial displacement and axial force of the bar using the uniform distributions of nodes. In the implementation, the spacing between adjacent nodes ( $\Delta x/L$ ) is taken as 1/8, 1/16, 1/24; the highest-order of the basis functions  $n=2, 3, 4$ ; and the support size  $a= 2.1\Delta x, 2.6\Delta x$ , for  $n=2$  in Table 1,  $a= 3.1\Delta x, 3.6\Delta x$  for  $n=3$  in Table 2;  $a= 4.1\Delta x, 4.6\Delta x$  for  $n=4$  in Table 3. In comparison with the exact solutions, it is observed from Tables 1-3 that the accurate solutions are obtained when  $a \approx 2.6\Delta x$  is used in the case of  $n=2$ ,  $a \approx 3.1\Delta x$  in the case of  $n=3$ , and  $a \approx 4.1\Delta x$  in the case of  $n=4$ ; that the variation of the present solutions with the values of free-chosen parameter  $\alpha$  is minor, and the present solutions obtained using the normalized Gaussian with  $\alpha=0.3$  yield the best accuracy among those obtained using the normalized Gaussian with  $\alpha=0.4, 0.5$  and using the other weight functions; and that the error norms of the present solutions of both the maximum displacement and axial force of the bar, obtained using  $\Delta x=1/16$ ,  $\alpha = 0.3$ ,  $n=3$  and  $a=3.1\Delta x$ , is less than 0.8% in comparison with the exact solutions.

The support size must not remain constant in the cases of random and non-uniform distribution of nodes, and the suitable support size of each sampling node will be dependent upon a fixed number of nearest neighboring nodes ( $NI$ ) included in the support region. According to the results in Tables 1-3, we suggest that the appropriate support size for each sampling node is determined by including about  $(2n+1)$  nearest neighboring nodes (i.e.,  $NI \approx (2n+1)$  or  $NI \approx (2N_n - 1)$  in which  $N_n$  is the total number of basis functions). This guidance of  $NI \approx (2N_n - 1)$  has also been extended to the following multi-dimensional problems. Fig. 3 shows the convergence rate of the displacement and axial force in the cases of  $n=2, 3, 4$ . It is shown that the present solutions of horizontal displacement obtained using  $n=2$  and  $n=3$  yield the convergence rate  $R \approx 2.0$ . The convergence rate in the case of  $n=4$  is much improved, and is up to  $R \approx 4.0$ . Fig. 4 shows the present results for the distributions of horizontal displacement and axial force functions along the length direction of the bar using three different node-distributions (i.e., node distributions  $A, B$  and  $C$ ) in which node distribution  $A$  is uniform with  $\Delta x/L=1/8$ , node distributions  $B$  and  $C$  are non-uniform with three different spacing ( $\Delta x/L=1/16, 1/8$  and  $1/4$ ) through the whole bar domain, and a variant support size with a fixed value of  $NI=5$  for each sampling point and  $n=2$  are used. It is shown that the present DRK approximation-based collocation solution using either the uniform or non-uniform distribution of nodes is in good agreement with the exact solution; Moreover, the present solu-

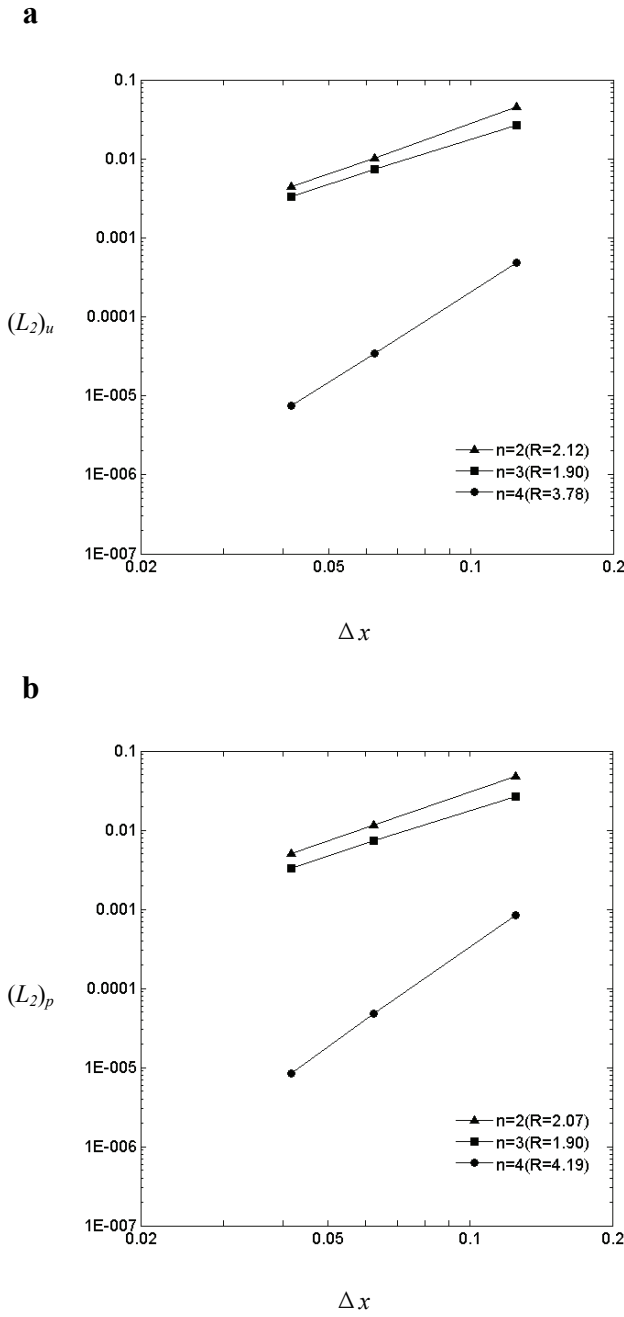


Figure 3: The convergence rate of the displacement and axial force in the cases of  $n=2, 3, 4$

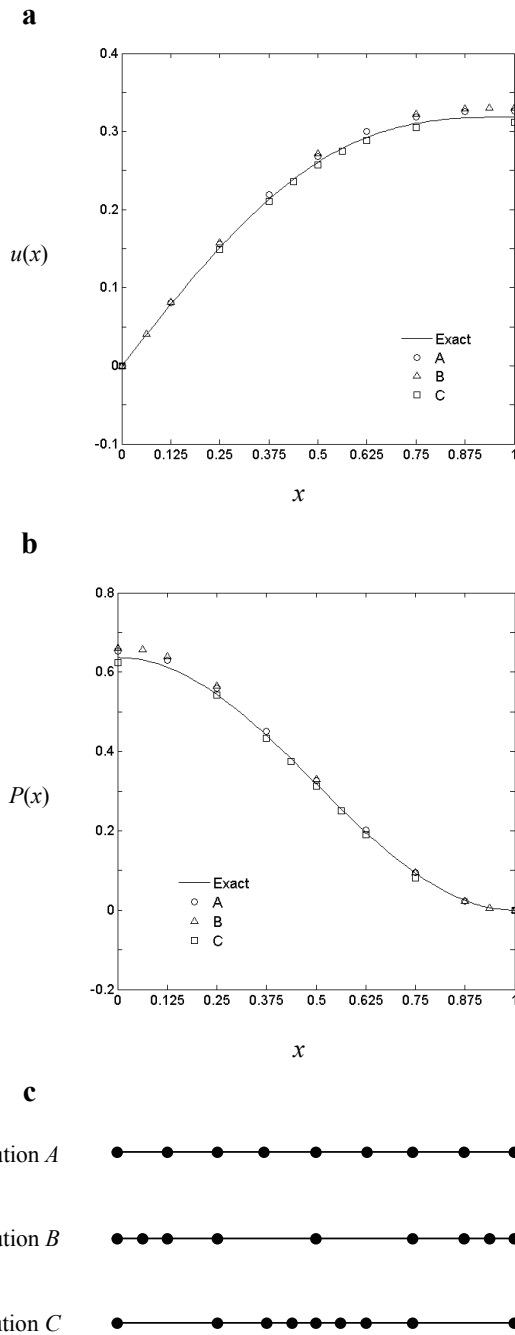


Figure 4: The present results for the distributions of horizontal displacement and axial force along the length direction of the bar using three different node-distributions

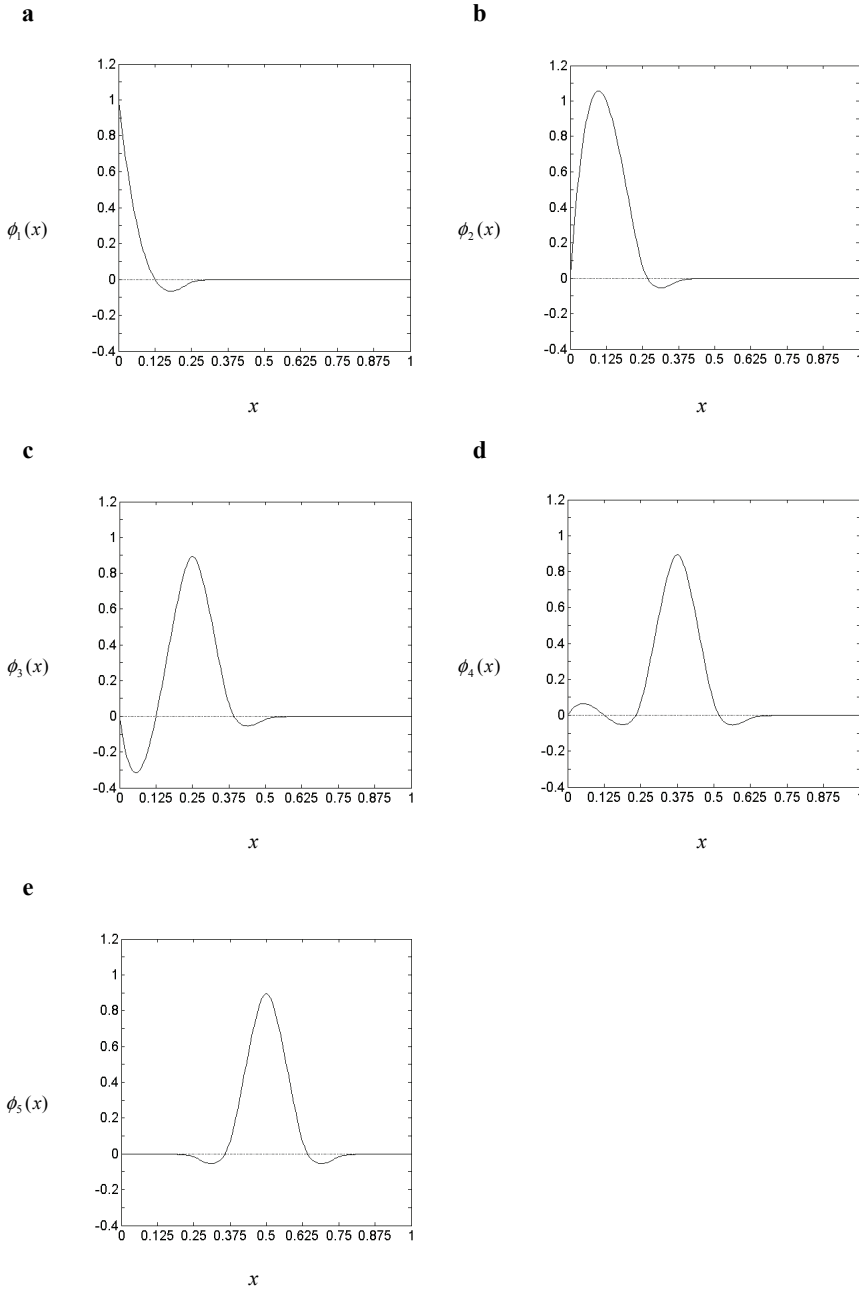


Figure 5: The through-length distributions of the shape functions for the RK approximant

tions are precisely satisfied both the essential boundary condition ( $u(0) = 0$ ) and the natural boundary condition ( $P(1) = 0$ ).

In order to have a clearer picture of the distributions of shape functions for the DRK approximant and its first-order and second-order derivatives along the bar domain, we present the through-length distribution of  $\phi_l(x)$  ( $l=1\sim 5$ ) and  $(\phi_5^{(1)}, \phi_5^{(2)})$  in Figs. 5 and 6, respectively. It is shown that these shape functions smoothly and continuously vary along the length coordinate of the bar.

#### 4.2 2D potential problems

A 2D potential problem governed by a Laplace equation in a square domain and associated with Dirichlet boundary conditions along the four edges is studied using the present DRK approximation-based collocation method. The problem was proposed and analyzed by Aluru (2000) using an RK approximation-based collocation method, and the governing equation for it is given as

$$\frac{\partial^2 \Phi}{\partial x^2} + \frac{\partial^2 \Phi}{\partial y^2} = 0 \quad 0 < x < 1, \quad 0 < y < 1, \quad (56)$$

where  $\Phi$  is the unknown function.

The boundary conditions on the four edges are prescribed as

$$\begin{aligned} \Phi(x=0) &= -y^3, & \Phi(x=1) &= -1 - y^3 + 3y^2 + 3y, \\ \Phi(y=0) &= -x^3, & \Phi(y=1) &= -1 - x^3 + 3x^2 + 3x. \end{aligned} \quad (57)$$

The exact solution is given as

$$\Phi(x, y) = -x^3 - y^3 + 3xy^2 + 3x^2y. \quad (58)$$

In the implementation, three sets of uniformly distributed nodes (5x5, 9x9 and 17x17) and a set of randomly distributed nodes (289 nodes) are used for the present analysis. Fig. 7 shows the node distributions in the square domain for a uniform distribution of (17x17) nodes and a random distribution of 289 nodes. Table 4 shows the present results of the unknown function ( $\Phi$ ) and its derivatives with respect to  $x$  and  $y$  (i.e.,  $\Phi_{,x}$  and  $\Phi_{,y}$ ) using the uniform distributions of (5x5), (9x9) and (17x17) nodes. The support size of each sampling node is considered to be variant, but the number of nearest neighboring nodes ( $NI$ ) included in this support domain of each sampling node remains the same, with  $NI$  taken to be 9, 11, 13 when  $n=2$ , and to be 17, 19, 21 when  $n=3$ . Because the exact solutions fall into the space spanned by

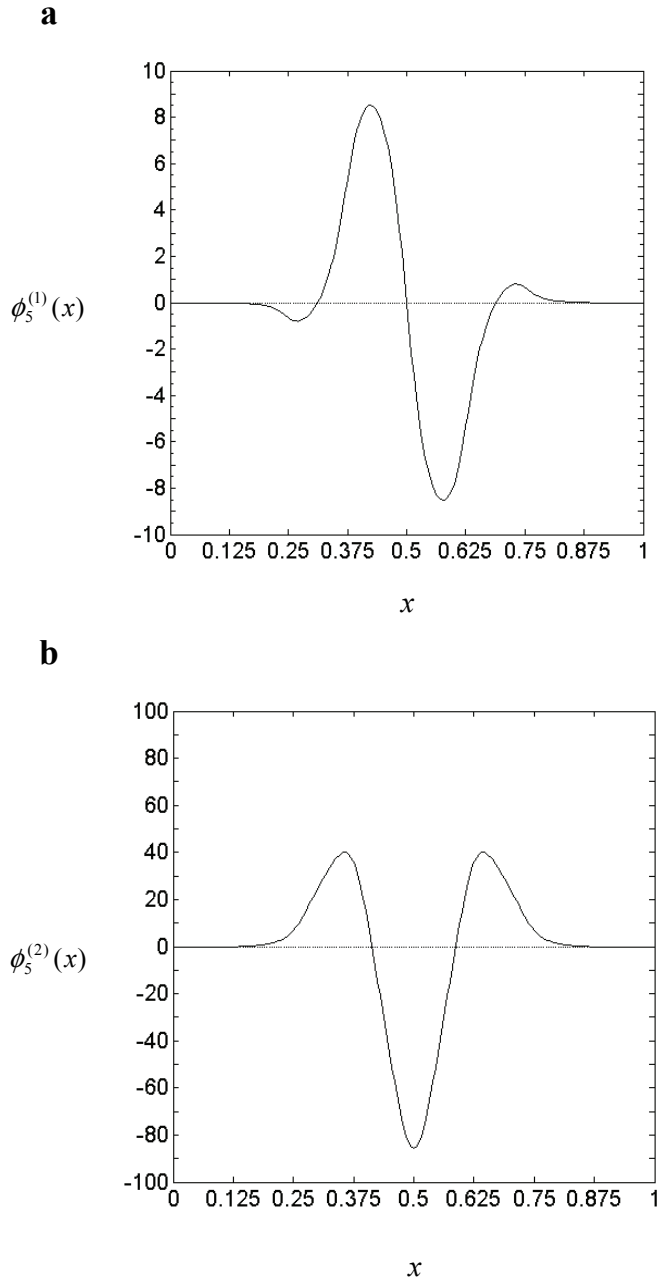


Figure 6: The through-length distributions of the shape functions for the first-order and second-order derivatives of the RK approximant

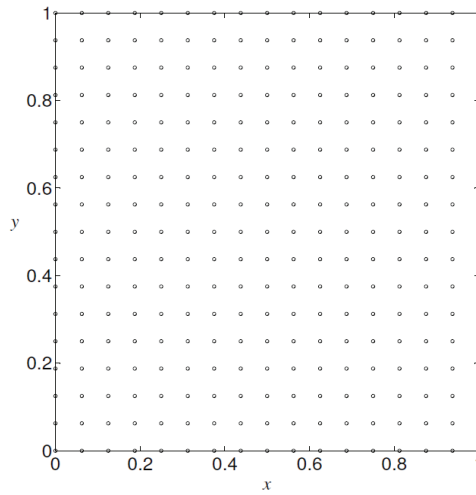
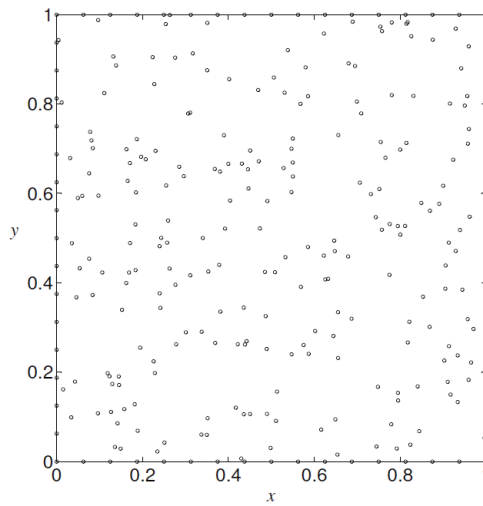
**a****b**

Figure 7: The node arrangements in the square domain for a uniform distribution of (17x17) nodes and a random distribution of 289 nodes

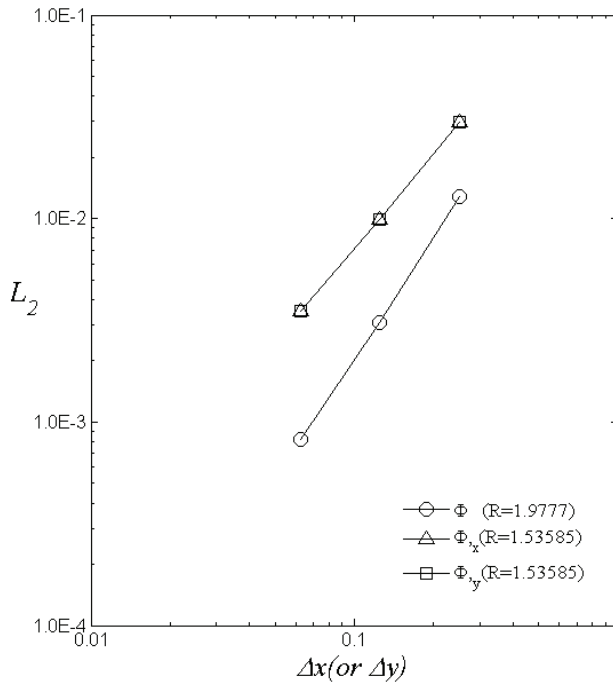


Figure 8: The rate of convergence of the unknown function and its derivatives for  $n=2$

the complete set of third-order basis functions ( $n=3$ ), it is seen in Table 4 that the present solutions with  $n=3$  are identical to the exact solutions in the cases of (5x5), (9x9) and (17x17) nodes; in the case of (9x9) nodes with  $n=2$  and  $NI=11$ , the relative errors of the unknown function and its derivatives is less than 1%. Fig. 8 shows the rate of convergence of the unknown function and its derivatives for  $n=2$ . It is shown that the rate of convergence ( $R$ ) is about 1.978 for  $\Phi$ , and about 1.536 for both  $\Phi_x$  and  $\Phi_y$ . The present solutions of ( $\Phi$ ,  $\Phi_x$  and  $\Phi_y$ ) at the 17x17 nodes, computed using a uniform distribution of (17x17) nodes and interpolated using the computed results of a random distribution of 289 nodes, are shown in Figs. 9–11, and it is found that both the computed and interpolated solutions are in excellent agreement with the exact solutions.

### 4.3 Plane elasticity problems

The present DRK approximation-based collocation method is further applied to a typical patch test of plane elasticity problems, as well as the problem of an infi-

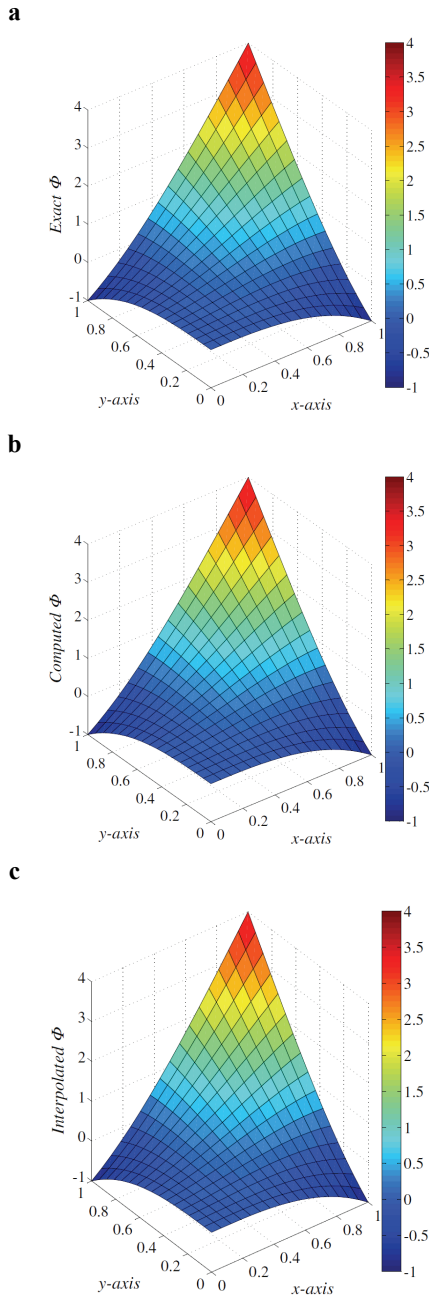


Figure 9: The present solution of  $\Phi$  using a uniform distribution of (17x17) nodes and a random distribution of 289 nodes

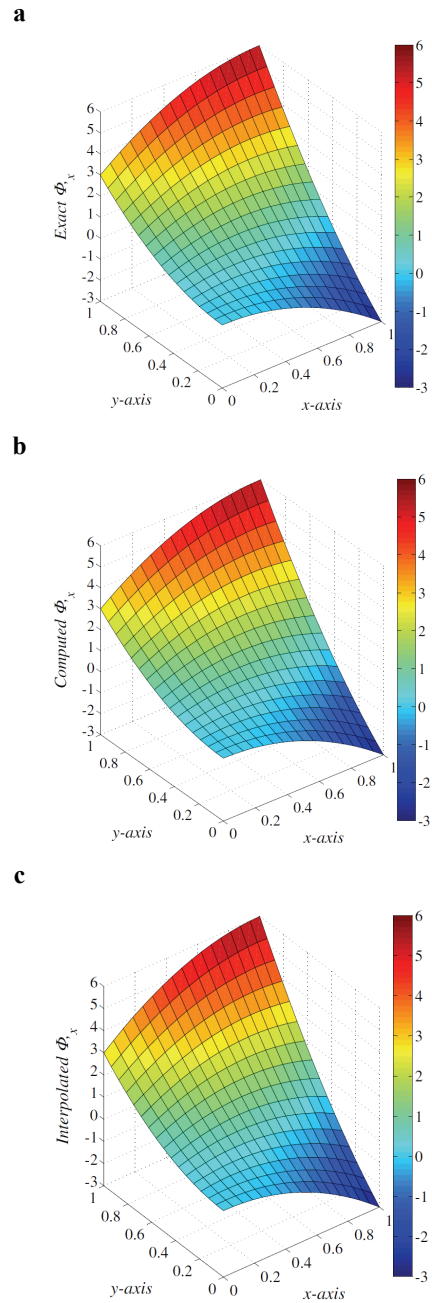


Figure 10: The present solution of  $\Phi_x$  using a uniform distribution of (17x17) nodes and a random distribution of 289 nodes

nite plate with a central hole where the material properties of the plane bodies are considered to be homogeneous and isotropic. The governing equations of plane elasticity in terms of the displacement components in the  $x$  and  $y$  directions are given as follows:

$$c_{11} u_{,xx} + c_{33} u_{,yy} + (c_{12} + c_{33}) v_{,xy} = 0, \quad (59)$$

$$(c_{12} + c_{33}) u_{,xy} + c_{33} v_{,xx} + c_{22} v_{,yy} = 0, \quad (60)$$

where  $u$  and  $v$  denote the displacement components in the  $x$  and  $y$  directions, respectively; and  $c_{ij}$  ( $i, j=1,2,3$ ) are the elastic stiffness coefficients.

The possible boundary conditions at each point on the boundary edge are

$$\text{either } (c_{11} u_{,x} + c_{12} v_{,y}) n_x + c_{33} (u_{,y} + v_{,x}) n_y = \hat{t}_x \text{ or } u = \hat{u}, \quad (61a)$$

$$\text{either } c_{33} (u_{,y} + v_{,x}) n_x + (c_{12} u_{,x} + c_{22} v_{,y}) n_y = \hat{t}_y \text{ or } v = \hat{v}, \quad (61b)$$

where  $n_x$  and  $n_y$  are the direction cosines of the unit vector relative to the given coordinates;  $\hat{t}_x$  and  $\hat{t}_y$  are the traction components; and  $\hat{u}$  and  $\hat{v}$  are the prescribed displacement components.

#### 4.3.1 Patch test

A patch test of plane elasticity problems is considered (Oñate, Perazzo and Miquel, 2001). In the patch test, a rectangular plate for which the in-plane dimensions are  $6 \times 12$  units is subjected to a uniform tensile stress with the magnitude of one at two edges in the  $x$  direction and is shown in Fig. 12. A quarter-plate model is used for the present analysis. The material properties of the plate are given as  $E=1$  and  $\nu=0.25$ . The exact solutions are  $u = x$ ,  $v = -y/4$ ,  $\sigma_x = 1$  and  $\sigma_y = \tau_{xy} = 0$ . Fig. 13 shows the node arrangements of a uniform distribution of nodes ( $4 \times 7$ ) and a random distribution of 28 nodes. Because the exact solutions fall in the space spanned by the complete sets of one-order, two-order or higher-order basis functions, the present solutions with  $n=1, 2$  or any other positive integer should lead to the exact solutions using the uniform distribution of  $4 \times 7$  and random distribution of 28 nodes. As expected, Table 5 shows the present solutions with a random distribution of 28 nodes and  $n=2$  coincide precisely with the exact solutions. Figs. 14–15 show the present solutions of in-plane displacements at the  $4 \times 7$  nodes which are computed using a uniform distribution of ( $4 \times 7$ ) nodes and interpolated using the computed results of a random distribution of 28 nodes. Again, it is noted that both the computed and interpolated solutions coincide precisely with the exact solutions. Based on the results of Table 5 and Figs. 14-15, we may conclude that the present DRK approximation-based collocation method passes the patch test of 2D plane elasticity, which is commonly used to validate the feasibility of a new numerical method in the literature.

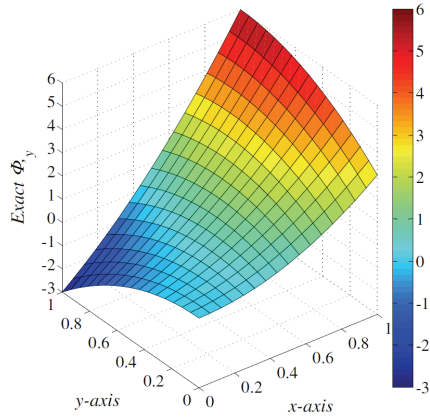
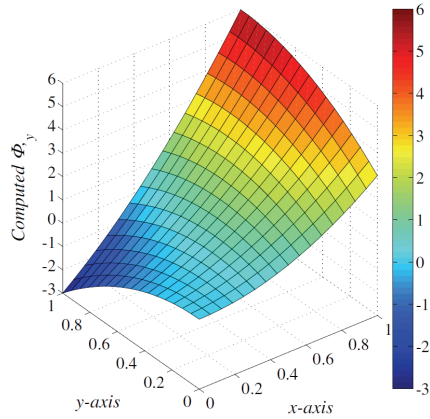
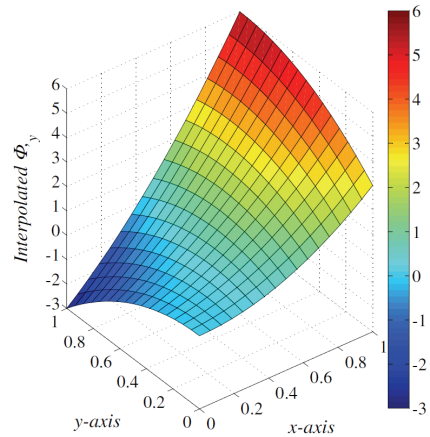
**a****b****c**

Figure 11: The present solution of  $\Phi_y$  using a uniform distribution of (17x17) nodes and a random distribution of 289 nodes

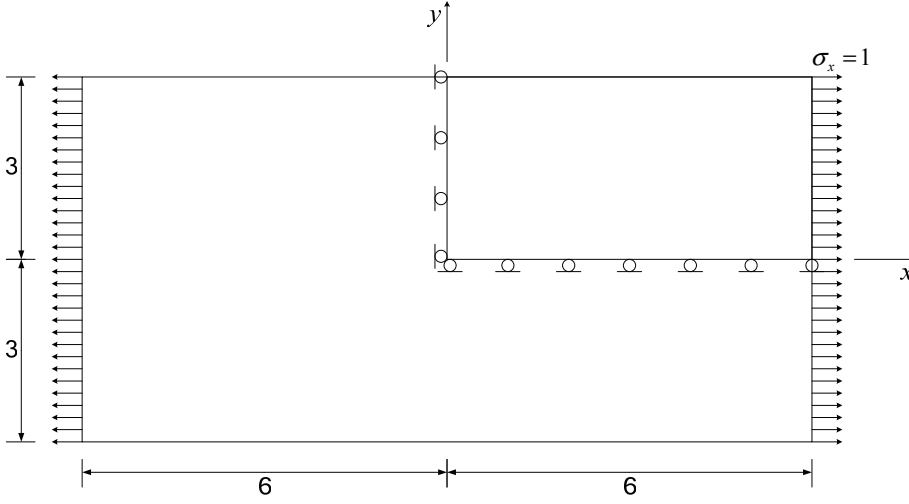


Figure 12: The configuration, coordinates and loading condition of a rectangular plate in a patch test

#### 4.3.2 Infinite plate with a circular hole

An infinite plate with a central hole of radius  $a$  ( $a=1\text{m}$ ) and subjected to a uniformly distributed traction  $\sigma_0$  ( $\sigma_0=1\text{N/m}^2$ ) in the  $x$  direction, is considered and shown in Fig. 16. The material properties are assumed to be homogeneous and isotropic and given as  $E = 1000 \text{ N/m}^2$  and  $\nu=0.3$ . The exact solutions for stress components are given as

$$\sigma_x = \sigma_0 \left[ 1 - \frac{a^2}{r^2} \left( \frac{3}{2} \cos 2\theta + \cos 4\theta \right) + \frac{3a^4}{2r^4} \cos 4\theta \right], \quad (62a)$$

$$\sigma_y = \sigma_0 \left[ -\frac{a^2}{r^2} \left( \frac{1}{2} \cos 2\theta - \cos 4\theta \right) - \frac{3a^4}{2r^4} \cos 4\theta \right], \quad (62b)$$

$$\tau_{xy} = \sigma_0 \left[ -\frac{a^2}{r^2} \left( \frac{1}{2} \sin 2\theta + \sin 4\theta \right) + \frac{3a^4}{2r^4} \sin 4\theta \right], \quad (62c)$$

where  $(r, \theta)$  are the polar coordinates and  $\theta$  is measured from the positive  $x$  axis counterclockwise.

The present DRK approximation-based collocation method is used to solve this problem, where a quarter-plate model is used due to symmetry. In the present analysis, three different non-uniform distributions of  $(NP \times NP)$  nodes are considered,

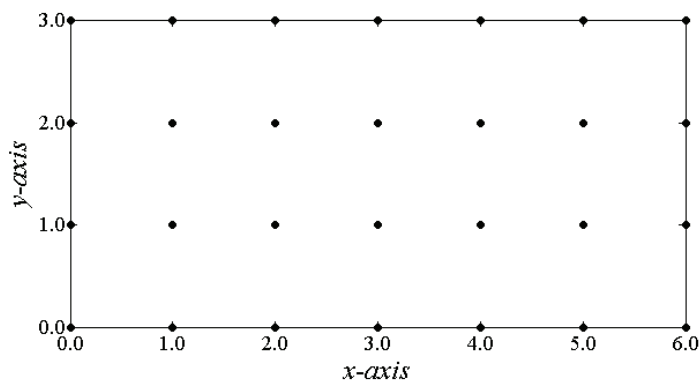
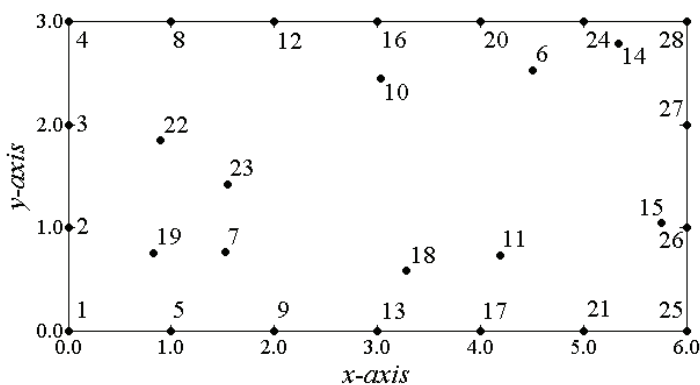
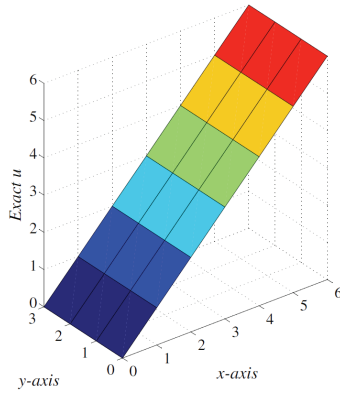
**a****b**

Figure 13: The node arrangements in the rectangular domain for a uniform distribution of (4x7) nodes and a random distribution of 28 nodes

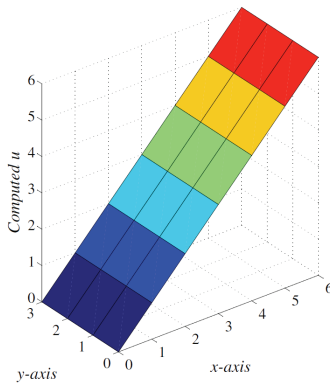
Table 6: The magnitudes of in-plane stress  $\sigma_x$  at point ( $r=1.0$ ,  $\theta = 90^0$ ) calculated using the distributions of (13x13), (15x15) and (17x17) nodes.

Distributions of nodes	$n$	$NI$	$\sigma_x$	$(L_2)_\Pi$
13×13	3	26	2.5726	7.57e-03
15×15	3	26	2.7805	4.12e-03
17×17	3	26	2.9384	2.32e-03
Exact solutions			3.0000	

**a**



**b**



**c**

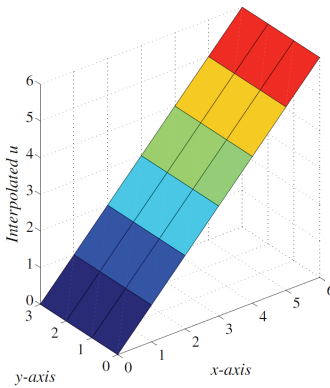
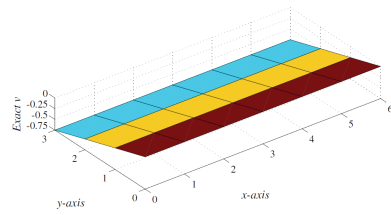
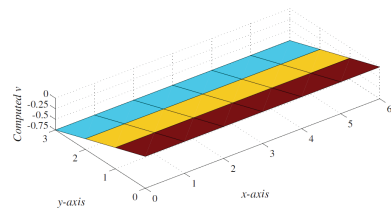


Figure 14: The present solution of  $u$  using a uniform distribution of (4x7) nodes and a random distribution of 28 nodes

**a**



**b**



**c**

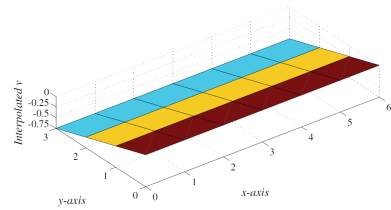


Figure 15: The present solution of  $v$  using a uniform distribution of (4x7) nodes and a random distribution of 28 nodes

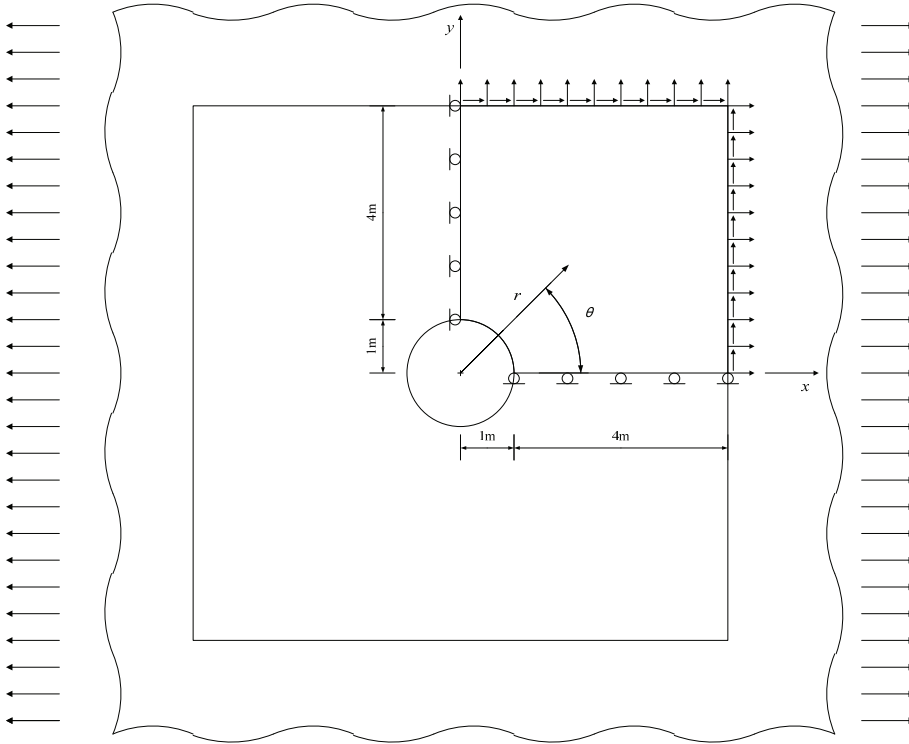


Figure 16: The configuration, coordinates and loading condition of an infinite plate with central hole

where  $NP = 13, 15, 17$ ; and the node arrangements are  $\Delta\theta = \pi/2(NP - 1)$  and  $r_i = 1 + [(i - 1)/(NP - 1)]^2(5 - 1)$ , ( $i = 1, 2, \dots, NP$ ) in the  $r$  and  $\theta$  directions, respectively. The node arrangement of the distribution of (17x17) nodes is shown in Fig. 17, in which the spacing between adjacent nodes is taken to be smaller, when the nodes become close to the hole. Fig. 18 shows the distribution of the stress component  $\sigma_x$  along the left edge ( $x=0$  and  $1\text{ m} < y < 5\text{ m}$ ). It is shown that the present solutions obtained using the distributions of both (15x15) and (17x17) nodes are in good agreement with the exact solutions, and the present (17x17)-node solutions are slightly more accurate than those of (15x15)-node solutions. Table 6 shows both the magnitudes of the in-plane stress  $\sigma_x$  at a crucial position ( $r=1\text{m}$ ,  $\theta = 90^\circ$ ) and the relative errors of the strain energy of the quarter plate using the distributions of (13x13), (15x15) and (17x17) nodes. The present solutions of the stress concentration factor ( $\sigma_x/\sigma_0$ ) at the point ( $r=1.0$ ,  $\theta = 90^\circ$ ), which is obtained using the non-uniform distributions of (13x13), (15x15), (17x17) nodes, are 2.5726,

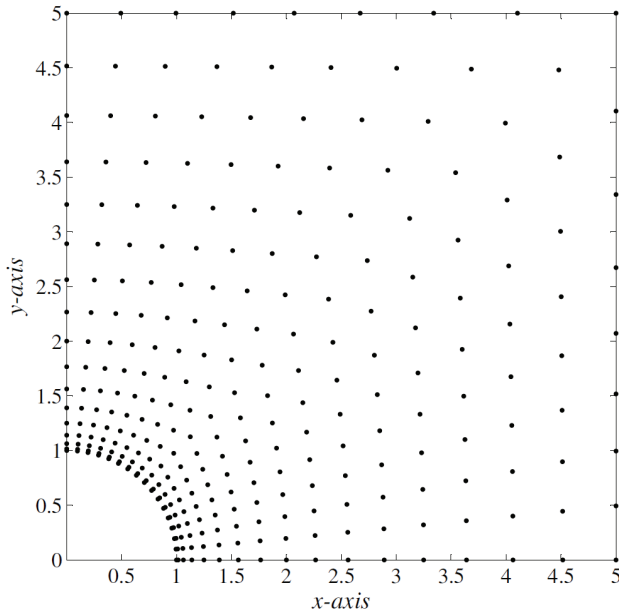


Figure 17: The node arrangement of a non-uniform distribution of (17x17) nodes

2.7805 and 2.9384, respectively. The stress concentration factor obtained using the distribution of (17x17)-nodes are 2,9384 are in good agreement with the exact solution which is 3, and its associated error norm of the strain energy of the quarter plate is 0.23%.

## 5 Concluding remarks

A DRK approximation-based collocation method has been proposed for solving the physical problems governed by the ordinary or partial differential equations with a set of appropriate boundary conditions. Unlike the conventional RK approximation, in which directly differentiating the shape functions of RK approximants was used to obtain the derivatives of RK approximants, we constructed a set of differential reproducing conditions to achieve this. The present DRK approximation-based collocation method has been applied to some one- and two-dimensional problems to validate its performance with regard to the static behavior of bars, a two-dimensional potential problem, a typical patch test of plane elasticity problems and an infinite plate with a central circular hole. It is shown that the present DRK approximation-based collocation method can be readily used to determine the derivatives of RK approximants, and the present DRK approximation solutions are

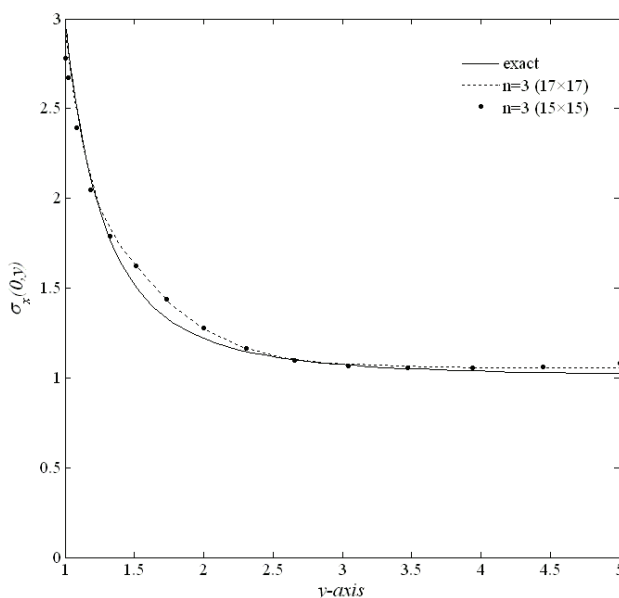


Figure 18: The distribution of the in-plane stress component ( $\sigma_x$ ) along the edge ( $x=0$  and  $1m < y < 5m$ )

very close to the available exact solutions with a rapid rate of convergence. Some guidance for using this method was also presented in this work. Specifically, the highest-order of basis functions used was suggested to be one or two orders higher than the highest-order of the governing equations. In addition, the support size for each sampling node was suggested to include about  $(2N_n - 1)$  nearest neighboring nodes for one-dimensional bar problems and two-dimensional potential problems, while for plane elasticity problems, the optimal values of  $NI$  will be larger than the earlier suggested value (i.e.,  $NI > 2N_n - 1$ ). In the case of  $n=3$ , the optimal values of  $NI$  are  $NI=7$  for one-dimensional bar problems,  $NI=19$  for two-dimensional potential problems, and  $NI=26$  for plane elasticity problems.

**Acknowledgement:** This work was supported by the National Science Council of Republic of China through Grant NSC 97-2221-E006-128-MY3.

## References

**Aluru, N.R.** (2000): A point collocation method based on reproducing kernel approximations. *International Journal for Numerical Methods in Engineering*, vol.

47, pp. 1083–1021.

**Atluri, S.N.** (2004): The Meshless Local Petrov-Galerkin (MLPG) Method for Domain & Boundary Discretizations, Tech Science Press, 700 pages, Forsyth, GA.

**Atluri, S.N.; Cho, J.Y.; Kim, H.G.** (1999): Analysis of thin beams, using the meshless local Petrov-Galerkin method, with generalized moving least squares interpolations. *Computational Mechanics*, vol. 24, pp. 334–347.

**Atluri, S.N.; Liu, H.T.; Han, Z.D.** (2006a): Meshless local Petrov-Galerkin (MLPG) mixed collocation method for elasticity problems. *CMES: Computer Modeling in Engineering & Sciences*, vol. 14, pp. 141–152.

**Atluri, S.N.; Liu, H.T.; Han, Z.D.** (2006b): Meshless local Petrov-Galerkin (MLPG) mixed finite difference method for solid mechanics. *CMES: Computer Modeling in Engineering & Sciences*, vol. 15, pp. 1–16.

**Atluri, S.N.; Shen, S.** (2002): The Meshless Local Petrov-Galerkin (MLPG) Method. Tech Science Press, 429 pages, New York, USA.

**Atluri, S.N.; Zhu, T.** (1998): A new meshless local Petro-Galerkin (MLPG) approach in computational mechanics. *Computational Mechanics*, vol. 22, pp. 117–127.

**Belinha, J.; Dinis, L.M.J.S.** (2006): Analysis of plates and laminates using the element-free Galerkin method. *Computers & Structures*, vol. 84, pp. 1547–1559.

**Belytschko, T.; Krongauz, Y.; Organ, D.; Fleming, M.; Krysl, P.** (1996): Meshless methods: An overview and recent developments. *Computer Methods in Applied Mechanics and Engineering*, vol. 139, pp. 3–47.

**Belytschko, T.; Lu, Y.Y.; Gu, L.** (1994): Element-Free Galerkin Methods. *International Journal for Numerical Methods in Engineering*, vol. 37, pp. 229–256.

**Chen, J.S.; Pan, C.; Wu, C.T.** (1997): Large deformation analysis of rubber based on a reproducing kernel particle method. *Computational Mechanics*, vol. 19, pp. 211–227.

**Chen, J.S.; Pan, C.; Wu, C.T.; Liu, W.K.** (1996): Reproducing kernel particle methods for large deformation analysis of non-linear structures. *Computer Methods in Applied Mechanics and Engineering*, vol. 139, pp. 195–227.

**Chen, J.S.; Yoon, S.; Wang, H.P.; Liu, W.K.** (2000): Improved reproducing kernel particle method for nearly incompressible finite elasticity. *Computer Methods in Applied Mechanics and Engineering*, vol. 181, pp. 117–145.

**Dai, K.Y.; Liu, G.R.; Han, X.; Lim, K.M.** (2005): Thermomechanical analysis of functionally graded material (FGM) plates using element-free Galerkin method. *Computers & Structures*, vol. 83, pp. 1487–1502.

**Han, Z.D.; Atluri, S.N.** (2004a): Meshless local Petrov-Galerkin (MLPG) approaches for solving 3D problems in elasto-statics. *CMES: Computer Modeling in Engineering & Sciences*, vol. 6, pp. 169–188.

**Han, Z.D.; Atluri, S.N.** (2004b): Meshless local Petrov-Galerkin (MLPG) approaches for solving 3D problems in elasto-dynamics. *CMC: Computers, Materials, & Continua*, vol. 1, pp. 129–140.

**Han, Z.D.; Rajendran, A.M., Atluri, S.N.** (2005): Meshless local Petrov-Galerkin (MLPG) approaches for solving nonlinear problems with large deformation and rotation. *CMES: Computer Modeling in Engineering & Sciences*, vol. 10, pp. 1–12.

**Jin, X.; Li, G.; Aluru, N.R.** (2005): New approximations and collocation schemes in the finite cloud method. *Computers & Structures*, vol. 83, pp. 1366–1385.

**Lancaster, P.; Salkauakas, K.** (1981): Surfaces generated by moving least squares methods. *Mathematics of Computation*, vol. 37, pp. 141–158.

**Libersky, L.D.; Petschek, A.G.; Carney, T.C.; Hipp, J.R.; Allahdadi, F.A.** (1993): High strain Lagrangian hydrodynamics—a three-dimensional SPH code for dynamic material response. *Journal of Computational Physics*, vol. 109, pp. 67–75.

**Liew, K.M.; Ng, T.Y.; Wu, Y.C.** (2002): Meshfree method for large deformation analysis—a reproducing kernel particle approach. *Engineering Structures*, vol. 24, pp. 543–551.

**Liew, K.M.; Wang, J.; Ng, T.Y.; Tan, M.J.** (2004): Free vibration and buckling analyses of shear-deformable plates based on FSDT meshfree method. *Journal of Sound and Vibration*, vol. 276, pp. 997–1017.

**Liu, G.R.** (2003): *Meshfree Methods: Moving beyond the Finite Element Method*. CRC Press, 691 pages, New York, USA.

**Liu, W.K.; Jun, S.; Li, S.; Adee, J.; Belytschko, T.** (1995): Reproducing kernel particle methods for structural dynamics. *International Journal for Numerical Methods in Engineering*, vol. 38, pp. 1655–1679.

**Liu, W.K.; Jun, S.; Zhang, Y.F.** (1995): Reproducing kernel particle methods. *International Journal for Numerical Methods in Engineering*, vol. 20, pp. 1081–1106.

**Lu, Y.Y.; Belytschko, T.; Gu, L.** (1994): A new implementation of the element free Galerkin method. *Computer Methods in Applied Mechanics and Engineering*, vol. 113, pp. 397–414.

**Lucy, L.** (1977): A numerical approach to testing the fission hypothesis. *Astrophysics Journal*, vol. 82, pp. 1013–1024.

**Monaghan, J.J.** (1988): An introduction to SPH. *Computational Physics Communications*, vol. 48, pp. 89–96.

**Nguyen, V.P.; Rabczuk, T.; Bordas, S.; Duflot, M.** (2008): Meshless methods: A review and computer implementation aspects. *Mathematics and Computers in Simulation*, vol. 79, pp. 763–813.

**Oñate, E.; Perazzo, F.; Miquel, J.** (2001) A finite point method for elasticity problems. *Computers & Structures*, vol. 79, pp. 2151–2163.

**Wu, C.P.; Chiu, K.H.; Wang, Y.M.** (2008a): A differential reproducing kernel particle method for the analysis of multilayered elastic and piezoelectric plates. *CMES: Computer Modeling in Engineering & Sciences*, vol. 27, pp. 163–186.

**Wu, C.P.; Chiu, K.H.; Wang, Y.M.** (2008b): A meshfree DRK-based collocation method for the coupled analysis of functionally graded magneto-electro-elastic shells and plates. *CMES: Computer Modeling in Engineering & Sciences*, vol. 35, pp. 181–214.

**Wu, C.P.; Chiu, K.H.; Wang, Y.M.** (2008c): A review on the three-dimensional analytical approaches of multilayered and functionally graded piezoelectric plates and shells. *CMC: Computers, Materials, & Continua*, vol. 8, pp. 93–132.

**Zhao, X.; Liew, K.M.; Ng, T.Y.** (2003): Vibration analysis of laminated composite cylindrical panels via a meshfree approach. *International Journal of Solids and Structures*, vol. 40, pp. 161–180.

**Zhao, X.; Ng, T.Y.; Liew, K.M.** (2004): Free vibration of two-side simply-supported laminated cylindrical panels via the mesh-free kp-Ritz method. *International Journal of Mechanical Sciences*, vol. 46, pp. 123–142.

**Zhou, J.X.; Zhang, H.Y.; Zhang, L.** (2005): Reproducing kernel particle method for free and forced vibration analysis. *Journal of Sound and Vibration*, vol. 279, pp. 389–402.

